MASTERARBEIT | MASTER'S THESIS

Titel | Title

Chromosome Configuration, Segregation, and Ploidy in the Euryarchaea Methanobrevibacter smithii and Methanopyrus kandleri

verfasst von | submitted by

Andrew Yang King

angestrebter akademischer Grad | in partial fulfilment of the requirements for the degree of

Master of Science (MSc)

Wien | Vienna, 2025

Studienkennzahl lt. Studienblatt	Degree programme code as it appears on the student record sheet:	UA 066 865
Studienrichtung lt. Studienblatt	Degree programme as it appears on the student record sheet:	Masterstudium Molecular Biology
Betreut von	Supervisor:	Mag. Mag. Dr.techn. Simon Karl-Maria Rasso Rittmann Privatdoz. Bakk.
Mitbetreut von	Co-Supervisor:	Mag. Nika Pende MSc PhD

Table of Contents

Contents

Table of Figures

Acknowledgements

First, I would like to sincerely thank Privatdoz. Dr. Simon K.-M. R. Rittmann for allowing me to join his laboratory group. I would also like to express my gratitude for being under the mentorship of my co-supervisor Dr. Nika Pende. Working with Dr. Rittmann and Dr. Pende helped me grow my abilities significantly as a scientist and independent researcher.

Second, I would like to express my gratitude to Assoc. Prof. Dr. Silvia Bulgheresi for her contributions in writing this master's thesis alongside Dr. Rittmann. I would also like to express my appreciation for receiving regular guidance from her during my time in the lab and for the privilege of collaborating with her group.

Thirdly, the Environmental Cell Biology laboratory group run by Prof. Bulgheresi helped me in developing my first protocols for many of my experiments, therefore I would like to express my thanks for this. Specifically, I would like to thank Nicole Krause M.Sc. for help in adapting the DNA Direct-geneFISH protocol to my archaeon. For help with bioinformatics (GC skew analysis and mark frequency analysis) and initial development of the qPCR protocol, I would like to thank Dr. Tobias Viehboeck.
I would like to give special thanks to Prof. Dr. Jörg Soppa at the Goethe University in Frankfurt, Germany for helping to optimize the qPCR.

Lastly, I would like to thank the entire Archaea Biology and Ecogenomics department for their support. This includes the many post-docs, PhD students, and lab technicians within the lab. Without a large support group, I would not have been able to accomplish as much as I did in the lab.

Abstract

The expansion of research on archaea, since its classification into its own domain in 1990, has created many new research opportunities. As we continue to find ways to combat climate change, methanogenic archaea have become of particular interest to researchers. This thesis investigates the chromosome biology of two non-model methanogen species, *Methanobrevibacter smithii* and *Methanopyrus kandleri*, focusing on chromosome configuration, segregation, and ploidy. Several state-of-the-art methods were used including Direct-geneFISH, RASER-FISH, qPCR, GC skew analysis, and marker frequency analysis (MFA). The chromosome of *M. smithii* was found to be monoploid, making it the first known monoploid among the Euryarchaeota. Preliminary results suggest that *M. kandleri* may be polyploid, although its chromosome configuration and segregation remain to be determined. These findings contribute to a deeper understanding of archaeal genome organization and may inform broader studies of microbial evolution and adaptation.

German Abstract

Mit zunehmender Forschung an Archaeen, seit ihrer Klassifizierung als eigene Domäne im Jahr 1990, haben sich zahlreiche neue wissenschaftliche Möglichkeiten eröffnet. Im Zuge der Suche nach Lösungen zur Bekämpfung des Klimawandels rücken methanogene Archaeen zunehmend in den Fokus der Forschung. Diese Arbeit untersucht die Chromosomenbiologie zweier nicht-modellhafter methanogener Spezies, *Methanobrevibacter smithii* und *Methanopyrus kandleri*, mit besonderem Augenmerk auf Chromosomenkonfiguration, -segregation und Ploidie. Dabei kamen mehrere moderne Methoden zum Einsatz, darunter Direct-geneFISH, RASER-FISH, qPCR, GC-Skew-Analyse und Markerfrequenzanalyse (MFA). Es konnte gezeigt werden, dass das Chromosom von *M. smithii* monoploid ist, womit es das erste bekannte monoploide Mitglied der Euryarchaeota darstellt. Vorläufige Ergebnisse deuten darauf hin, dass *M. kandleri* polyploid sein könnte, obwohl die genaue Chromosomenkonfiguration und -segregation noch nicht bestimmt werden konnten. Diese Erkenntnisse tragen zu einem tieferen Verständnis der genomischen Organisation von Archaeen bei und könnten weiterführende Studien zur mikrobiellen Evolution und Anpassung unterstützen.

Introduction

Phylogenetic placement of methanogenic archaea

Thought to be more related to bacteria than eukaryotes, hence previously classified in the domain of Archaebacteria (Woese & Fox, 1977), Archaea have since 1990 been classified into their own domain of life (Woese et al., 1990). This domain is subdivided into the Euryarchaeota and Crenarchaeota (Woese et al., 1990). The Euryarchaeota is comprised of methanogens and their relatives. Within the large group of Euryarchaota lie the orders Methanobacteriales (containing non-motile methanogens with their membranes containing pseudomurein cell walls and C20 and C40 isopranyl glycerol ethers) and Methanopyrales (a novel group containing a single species that can grow at 110 °C) (Garcia et al., 2000; Huber et al., 1989). Within Methanobacteriales is the family of Methanobacteriacea and Methanothermacea. The Methanobacteriacea specifically includes the genera Methanobacterium, Methanothermobacter, Methanobrevibacter, and Methanosphaera. A particularly interesting species, abundant in sewage sludge, the intestinal tracks of animals, and in the human gut, *M. smithii* lies within the seven-member genus of *Methanobrevibacter* (Figure 1) (Miller & Wolin, 1986). Within the order Methanopyrales lies the singular species of the family Methanopyraceae and genus *Methanopyrus* (Figure 1), *M. kandleri* (Boone et al., 1993). It is completely unrelated to any other methanogens (Burggraf et al., 1991).

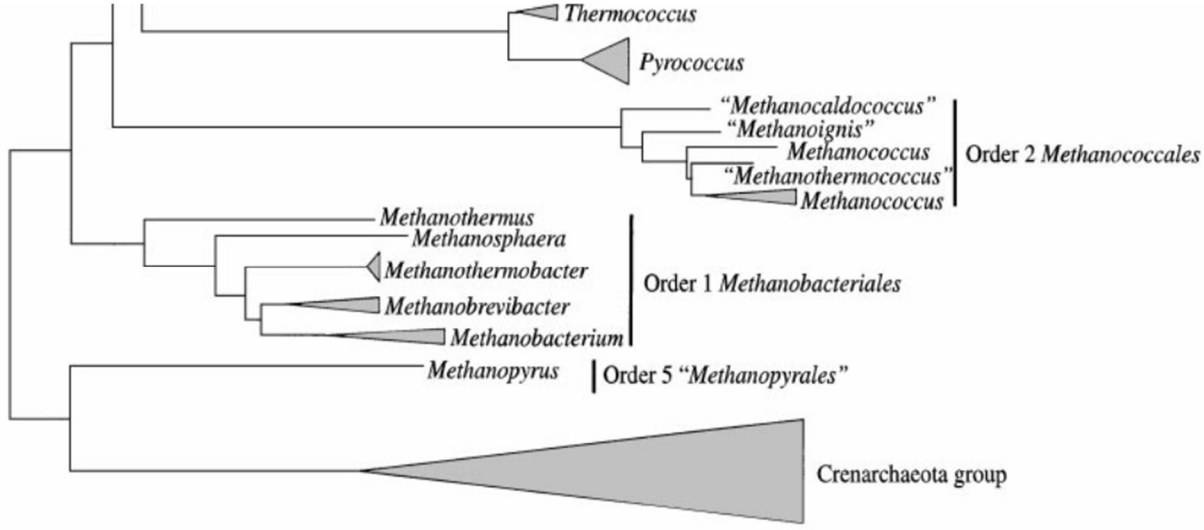

Figure 1 Phylogenetic tree of methanogens. Created by Garcia et al., 2000 and originally adapted from Boone et al., 1993.

Importance of methanogenic archaea in health, environment and biotechnology

As more research on methanogens is being pursued, many new implications have been revealed for ecology, biotechnology, and medicine. Ecologically, they play an important role in the global methane cycle on Earth (Conrad, 2009) but also in many complex microbiomes (Moissl-Eichinger et al., 2018). Methane is a key greenhouse gas, making

methanogenic archaea key greenhouse gas emitters. Methanogens also have many ecological impacts on a small scale within their microbiomes. They are a highly diverse group, however, they cannot utilize complex organic matter. Instead they only convert CO_2 (convert CO_2 and H_2 into methane), methyl-group-containing compounds, or acetate (Liu & Whitman, 2008). As a result, methanogens are highly dependent on other organisms, leading to their close association, typically with bacteria, particularly archaeal species like *M. smithii* that form symbiotic relationships in the human-gut microbiome (Djemai et al., 2022). Methanogens have a broad distribution, as they are viable at temperatures between 4-110 °C and have unique adaptations to their individual environments. Examples of the adaptable nature of the methanogens include hyperthermophiles like *M. kandleri* which exist near hydrothermal vents where the temperature is up to 110 °C (Kurr et al., 1991). There are also halophiles like *Haloferax volcanii* (previously known as *Halobacterium volcanii*), which have been isolated from the extremely high salt conditions of the Dead Sea (Mullakhanbhai & Larsen, 1975).

The ability for these archaea to fill ecological niches along with methanogenesis (production of methane from CO_2 and H_2) has sparked great interest in finding applications for them in the biotech industry. As the world tries to find alternatives to fossil fuels, methanogens could be utilized to produce methane for energy and biofuels (Ren et al., 2008). Methanogens also have many applications in the production of enzymes, polyhydroxybutyrate **(**PHB), and methanol (Strong et al., 2015). With advancements in genetics regarding methanogens, it is becoming easier than ever to adjust the production output of methanogens (Konisky, 1989).

Methanogens have also started to receive attention in medicine, since they could have implications on human health. One such archaeon is *M. smithii*, which is the dominant archaeon in the human gut (Samuel et al., 2007). One study quantified the concentration of *M. smithii* in the gut of malnourished children, finding a significant decrease of *M. smithii* in children with acute malnutrition (Camara et al., 2021). This suggests an important role of *M. smithii* in nutrition. Another study used quantitative polymerase chain reaction (qPCR) to quantify the amount of *M. smithii* in healthy patients and those with IBD (irritable bowel disease) (Ghavami et al., 2018). The results showed that healthy patients had a significantly higher amount of *M. smithii* than IBD patients, suggesting the importance of *M. smithii* on health. Furthermore, a study on childhood weight development revealed that obese children had significantly higher amounts of *M. smithii* compared to those not overweight, suggesting possible negative implications of overabundance of *M. smithii* in humans (Mbakwa et al., 2015).

Lack of fundamental research on chromosome biology in methanogens

Although there is a growing body of research surrounding methanogens, there is still a lack of fundamental research on them, specifically regarding their ploidy, chromosome organization and segregation. For cell biology, *Sulfolobales* species such as *S.*

acidocaldarius, *S. sulfataricus*, *S. toodaii*, and *S. islandicus* have become model organisms. This is a result of their genetic tractability, metabolic diversity and their importance in studying archaeal genome evolution (Grogan, 1989; Reno et al., 2009). Because of their fast growth (doubling time of 2 hours) (Leigh et al., 2011) and genetic tractability, *Methanococcus* species, specifically species like *M. maripaludis* have become model organisms. Two other genetically tractable model organisms are the halophilic archaea *Haloferax volcanii* and *Halobacterium salinarum*. They are easier to cultivate than *Methanococcus*, as they grow aerobically, while also having fast growth (J. L. Robinson et al., 2005).

What has become apparent is that the focus on emerging model organisms for archaeal studies has left a gap in fundamental knowledge of organisms that are not amenable to genetic manipulation. With respect to ploidy, current observations have been largely limited to model organisms, as illustrated in Figure 2 (Barillà, 2016). While the Euryarchaea and Crenarchaea exhibit remarkable diversity, their ploidy appears not to reflect this. The limited sample size, coupled with the fact that ploidy has only been characterized in model organisms, raises skepticism. Much like our understanding of the extensive ecological diversity within these two groups, we must ask: are we truly capturing the full range of ploidy diversity in archaea?

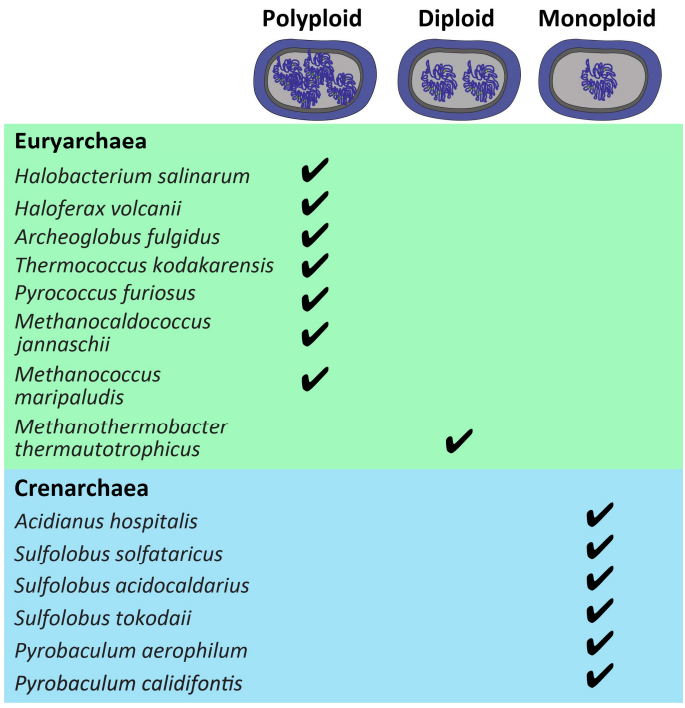

Figure 2 Table of organisms with known ploidy of Euryarchaea and Crenarchaea. Adapted by Nika Pende and originally from Barillà (2016).

Furthermore, almost no research has been done regarding the configuration or segregation of archaeal chromosomes. This contrasts with bacteria, which have extensive research regarding these topics. What we do understand is that archaeal genomes are organized in circular chromosomes with extrachromosomal elements

(plasmids) (Barillà, 2016). It has been observed, such as in halophilic Euryarchaea, that these plasmids are large (Capes et al., 2011), while in Crenarchaea these plasmids are small (Wang et al., 2015). Unlike in bacteria, it has been observed that archaea can harbor a chromosome containing one or more origins of replication (Lindås & Bernander, 2013; Lundgren et al., 2004; Norais et al., 2007; Wu et al., 2014). Also, in contrast to bacteria, the archaeal cell cycle has been observed to vary greatly, sharing many traits with both prokaryotic and eukaryotic cell cycles, and resulting in the use of eukaryotic cell cycle nomenclature (Barillà, 2016).

Regarding specific segregation studies, we know that Crenarchaea from the genus *Sulfolobus* have a prolonged G2 stage containing two chromosome copies and appearing as a single nucleoid (Bernander & Poplawski, 1997; Lundgren et al., 2008; Popławski & Bernander, 1997; N. P. Robinson et al., 2007). Segregation in *Sulfolobus* occurs rapidly followed by cytokinesis. The chromosome replication and segregation are strictly temporally separated (Popławski & Bernander, 1997; N. P. Robinson et al., 2007), suggesting faithful distribution of the chromosomes to the daughter cells is important in monoploid archaea (Barillà, 2016). In contrast to the Crenarchaea, members of the Euryarchaea, such as *Methanocaldococcus jannashii* (previously *Methanococcus jannashii)*, have been observed as polyploids and to have a very relaxed cell cycle (Malandrin et al., 1999). Cell division occurs asymmetrically and results in an uneven distribution of chromosome copies in daughter cells. The G2 stage is very brief, such as in *Methanothermobacter thermautotrophicus* (Majerník et al., 2005) or completely absent as sometimes is the case in *Methanoccous maripaludis* (Hildenbrand et al., 2011). As we can observe, archaea chromosome segregation is diverse and differs from both typical eukaryotic and prokaryotic cell division. Based on what we know so far, some hypotheses have been developed, such as linking monoploidy with a very strict cell cycle and polyploidy with a very relaxed cell cycle, and suggesting that the presence of histones is directly related with polyploidy in Euryarchaea (Sandman & Reeve, 2006; Spaans et al., 2015; White & Bell, 2002). It remains an issue though, that much of this research used to generate these hypotheses use a few model organisms. Will a broader knowledge of archaeal chromosome biology that includes non-model organisms confirm what concluded from studying a few model organisms?

Origin of replication

As previously mentioned, archaea can have one or multiple origins of replication (oriC) per chromosome as shown in Figure 3 (Wu et al., 2014). It has been observed that the oriC in archaea is composed of two elements seen in Figure 4. First is an AT-rich DNA unwinding element (DUE) (Mackiewicz et al., 2004), where initial opening of the DNA double helix occurs (Kowalski & Eddy, 1989), and flanked by several conserved repeated motifs called origin recognition boxes (ORBs) (N. P. Robinson et al., 2004). Second is the *orc1/cdc6* gene that encodes for the initiator protein. It is homologous to both the eukaryotic origin recognition complex (ORC) proteins and Cdc6 protein. These proteins are involved in recognition of the origin region and loading of the DNA helicase

minichromosome maintenance helicase (MCM) (Matsunaga et al., 2001; N. P. Robinson & Bell, 2005). Corresponding to the number of oriC, multiple paralogs of *orc1*/*cdc6* can be encoded and not all origins of replication are used, even if they are present, such as in *Sulfolobus acidocaldarius* (Duggin et al., 2008).

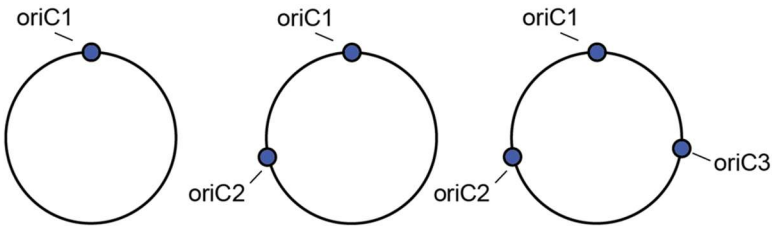

Figure 3 Representation of an archaeal chromosome with one, two, and three origins of replication. Made by Nika Pende.

Termination of replication

In archaea, additional to the oriC, there is a region located opposite to it in the genome known as the termination of DNA replication region (ter) where the two replication forks meet (Cortez et al., 2010). This is similar to bacteria such as *Escherichia coli*, where the oriC and ter are also positioned opposite to one another on the chromosome (Louarn et al., 1977; Reyes-Lamothe et al., 2012). In archaea, there are two closely associated ter elements: the tyrosine recombinase *xerA*, encoding a homologue of the bacterial XerCD (Cortez et al., 2010), and *dif* sites (Reyes-Lamothe et al., 2012), a substrate for homologous recombination by XerA (Serre et al., 2013). XerA resolves chromosome dimers at dif sites, during homologous recombination. There is not always a *dif* site for each ter as seen in Figure 4.

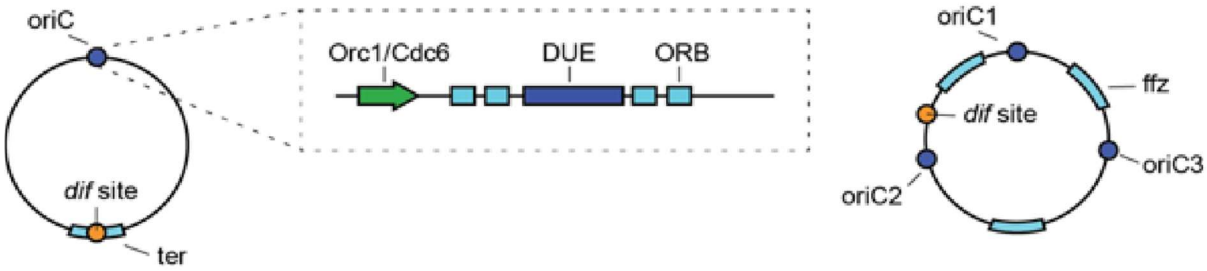

Figure 4 Representation of an archaeal chromosome with termination of replication elements. Adapted by Nika Pende and originally adapted from Lindås & Bernander, 2013.

Both the location of the oriC and ter together, seen in Figure 5, are used to determine the chromosome configuration.

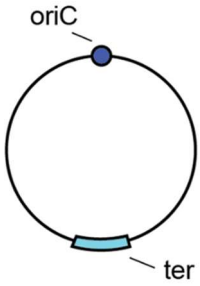

Figure 5 Typical position of the origin (oriC) and terminus (ter) of replication on an archaeal chromosome. Made by Nika Pende.

In bacteria, there are two established chromosomal configurations, longitudinal (oriC and ter are oppose along the long axis of the cell) and transverse (oriC and ter are opposite along the short axis the cell) (Figure 6).

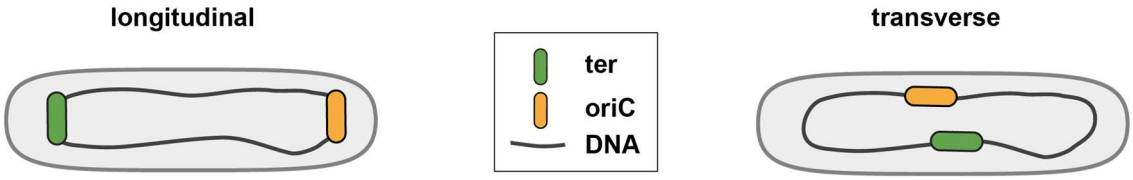

Figure 6 Two possible chromosome configurations. Adapted by Nika Pende originally from Weber et al. (2019).

The presence of archaeal peptidoglycan makes studying methanogens difficult

Methanogenic archaea from the orders of Methanopyrales and Methanobacteriales are particularly difficult to work with, due to the presence of a bacterial homologue of peptidoglycan (murein), termed archaeal peptidoglycan (pseudomurein), which makes up the cell membrane of these two methanogen orders (Albers & Meyer, 2011). Unlike murein, which has an *N*-acetyl-muramic acid with a β-1,4 linkage to N-Acetyl-D-glucosamine (NAG), pseudomurein has *N*-acetyl-L-talosaminuronic acid (NAT) with a β-1,3 linkage to NAG (Kandler & Konig, 1993). A consequence of this different structure is that species in these orders have membranes that cannot be lysed with lysozyme or other bacterial hydrolases (Visweswaran et al., 2010). This makes performing experiments like fluorescence in-situ hybridization (FISH) or immunolabeling difficult with these species. As a result, an enzyme termed pseudmurein endoisopeptidase (PEI) was derived, so far from two prophages from two methanogen species, *Methanothermobacter wolfeii* (PEIW) and *Methanothermobacter marbugensis* (PEIP) (Kubota et al., 2008; Pfister et al., 1998; Steenbakkers et al., 2006). Both PEIW and PEIP cleave the oligopeptides that link the sugar chains of adjacent pseudomurein layers between the ϵ-amino group of L-lysine and the carboxyl group of the L-alanine residue (Kiener et al., 1987; Luo et al., 2002). This has allowed researchers to work with methanogens from these orders to perform experiments like FISH (Kubota et al., 2008; Nakamura et al., 2006).

Limited methods available for studying chromosome biology in methanogenic archaea

The lack of research on non-model organisms and the unique characteristics of species, like in the orders Methanopyrales and Methanobacteriales, have resulted in a limited number of methods developed for studying these organisms, specifically regarding their chromosome biology. With the development of PEI and the natural expansion of research into archaea, there is however an increasing number of methods available. Some of these methods include: sequencing, biomarkers, qPCR, and various fluorescence in-situ hybridization (FISH) methods (catalyzed reporter deposition CARD, microautoradiography MAR, 16S RNA) (Kumar et al., 2011). For example, 16S RNA FISH was used to quantify the efficacy of the PEIW enzyme using four methanogens (*Methanobacterium bryantii*, *Methanobrevibacter ruminantium*, *Methanosphaera stadtmanae*, and *Methanothermobacter thermautotrophicus*), showing PEIW has high efficacy, but that it differs depending on the species (Nakamura et al., 2006). Another group performed CARD-FISH on 12 methanogens, to also test the efficacy of PEIW compared to traditional methods for bacteria such as lysozyme and proteinase K, showing what the previous study showed (Kubota et al., 2008). There are various types of FISH experiments, and it has many applications, many that have been applied to study the chromosome biology of bacteria. Consequently, these could also be used to study the chromosome biology in methanogens, however, this is an emerging field of archaea research. Beyond FISH, methods are being developed for the determination of ploidy using quantitative methods. Flow cytometry combined with epifluorescence microscopy was used to determine the ploidy of *Methanothermobacter thermautotrophicus*, which was observed as diploid (Majerník et al., 2005). In another study, qPCR was optimized to study the ploidy of *Methanosarcina acetivorans* and *Methanococcus maripaludis* (Hildenbrand et al., 2011). It was discovered that *M. acetivorans* had a polyploidy of 17 during fast growth and 3 during slow growth, while *M. maripaludis* was found to have a polyploidy of 55 in exponential and 30 in stationary. Another study on *Haloferax volcanii* also utilized qPCR to determine the ploidy at different conditions (Maurer et al., 2017). It was determined that *H. volcanii* is polyploid and has 20 genome copies in optimal growing conditions but can be as low as 2 during phosphate starvation or up to 40 under a phosphate surplus.

Goals

Using current knowledge, I sought to expand our understanding of archaeal chromosome biology, specifically that of methanogenic archaea. We still lack established methods to study this, particularly in non-model organisms. My first goal was to establish two new FISH protocols for *M. smithii* and *M. kandleri*, adapting one protocol used on bacteria (Direct-geneFISH) and another used on eukaryotes (RASER-FISH), to determine the chromosome configuration and segregation of these two species. In a broader context, this was done in the hopes it will open new opportunities for studies on more methanogenic archaea but also archaea as a whole, since neither

of these methods have yet been established for archaea. Furthermore, this will hopefully also establish the method for determining the chromosome configuration and segregation in non-model archaea. My second goal was to qualitatively compare the two FISH methods to determine which one provides better results for determining the chromosome configuration and segregation of the two methanogens. My third goal was to adapt a protocol, applied to halophilic archaea, for performing qPCR of single copy genes for both *M. smithii* and *M. kandleri*, to determine the ploidy of these two species. Both the Direct-geneFISH and RASER-FISH would help verify any results obtained from the qPCR.

Hypotheses

I hypothesize that the chromosome configuration and segregation of *M. smithii* and *M. kandleri* will be longitudinal. Of the two FISH methods, Direct-geneFISH and RASER-FISH, I hypothesize that RASER-FISH will provide the best results compared to Direct-geneFISH. Based on previous knowledge of archaeal ploidy, I hypothesize that *M. smithii* and *M. kandleri* will be polyploid.

Methods

Cultivation

Growing conditions

M. smithii and *M. kandleri*, referred to as methanogens here, were grown as closed batch cultures. The methanogens were grown under anaerobic conditions with a mixture of molecular hydrogen (H_2) and carbon dioxide (CO_2) containing 20 Vol.-% CO_2 in H_2 (H_2/CO_2). For autoclaving, to maintain anaerobic conditions of the medium, a mixture of molecular nitrogen (N_2) and CO_2 containing 20 Vol.-% CO_2 in N_2 (N_2/CO_2) was used. The methanogens were grown in 120 mL serum bottles with a crimped-on rubber stopper. *M. smithii* was incubated at 37 °C shaking at 120 RPM (Innova 44, New Brunswick Scientific, USA) while *M. kandleri* was incubated at 98 °C in a water bath at140 RPM (Water Bath Circulating 22L, Hach, USA). A mixture of H_2/CO_2 at a pressure of 2 bars was used to maintain the cultures of both methanogens. The growth of the cultures was monitored by using a manometer (LEO 1, Keller, Switzerland) every day to check for gas consumption. To check the quality of the cultures, samples were periodically viewed under phase contrast using an Eclipse NI-L microscope (Nikon, Japan). To maintain some cultures at exponential growth for specific use in DNA FISH experiments, transfers of each culture were made every few days from the previous culture. Excess cultures, not used for transfers, were stored at 4 °C and kept as backup cultures in case any issues were encountered during cultivation.

M. smithii medium

Medium

M. smithii was grown in an adapted DSMZ 141 methanogen medium containing 0.34 g KCl, 4 g $MgCl_2 \cdot 6H_2O$, 0.25 g NH_4Cl, 0.106 g $CaCl_2$, 0.14 g KH_2PO_4, 0.84 g $MgSO_4$, 6 g NaCl, 1 g sodium acetate, 2 g yeast extract, 10 mL of trace element solution, 2 mL of $Fe(II)(NH_4)_2(SO_4)_2 \cdot 6H_2O$ solution, and 0.5 mL of Na-resazurin solution (0.7 mg mL^{-1}), then brought to a total volume of 980 mL with MQ water. Next, 10 mL of vitamin solution, 5 g $NaHCO_3$, 0.5 g L-Cystein-HCl were added. Finally, the medium was filled up to a final volume of 1 L with MQ water (Pende et al. 2021). 50 mL of medium was then added to 120 mL serum bottles, closed with a rubber stopper, and sealed by crimping. The medium was flushed with 20 Vol.-% CO_2 in N_2, the pH adjusted to a pH of 7 and the bottles autoclaved at 121 °C (HV Series, Hirayama, Japan). After the bottles cooled down 0.2 mL of $Na_2S \cdot H_2O$ (0.61 mol L^{-1}) were added and the medium was flushed with H_2/CO_2. The medium was stored in a dark at room temperature.

TE Solution

The TE solution contained 1.5 g nitrilotriacetic acid, 3 g $MgSO_4 \cdot 7H_2O$, 585 mg $MnCl_2 \cdot 4H_2O$, 1 g NaCl, 100 mg $FeSO_4 \cdot 7H_2O$, 180 mg $CoSO_4 \cdot 7H_2O$, 100 mg $CaCl_2 \cdot 2H_2O$, 180 mg $ZnSO_4 \cdot 7H_2O$, 6 mg $CuSO_4$, 20 mg $KAl(SO_4)_2 \cdot 12H_2O$, 10 mg H_3BO_3, 10 mg $Na_2MoO_4 \cdot 2H_2O$, 30 mg $NiCl_2 \cdot 6H_2O$, 0.3 mg $Na_2SeO_3 \cdot 5H_2O$, 0.4 mg $NaWO_4 \cdot 2H_2O$, in 1 L of MQ water.

Vitamin Solution

The vitamin solution contained 2 mg biotin, 2 mg folic acid, 10 mg pyridoxine-HCl, 5 mg thiamine-HCl·$2H_2O$, 5 mg riboflavin, 5 mg nicotinic acid, 5 mg D-Ca-pantothenate, 0.1 mg vitamin B12, 5 mg p-aminobenzoic acid, 5 mg lipoic acid in 1 L of MQ water.

M. kandleri medium

Medium

M. kandleri was grown in DSMZ 511 medium containing 0.25 g NH_4Cl, 0.087 g K_2HPO_4, 0.09 g KH_2PO_4, 11.80 g NaCl, 1.75 g $MgSO_4 \cdot 7H_2O$, 4.5 g $MgCl_2 \cdot 6H_2O$, 0.81 g Na_2SO_4, 0.78 g $CaCl_2 \cdot 2H_2O$, 0.3 g KCl, 10 mL TE solution, 2 mL $(NH_4)_2Fe(SO_4)_2 \cdot 6H_2O$ solution (0.1% w/v), 2 mL $(NH_4)_2Ni(SO_4)_2$ solution (0.1% w/v), 2 mL $Na_2WO_4 \cdot 2H_2O$ solution (0.1% w/v), 10 mL Marine TE, 0.5 mL Na-resazurin solution (0.1% w/v), 1 g $NaHCO_3$, 10 mL vitamin solution (also used for *M. smithii* medium), in 1 L MQ water. 50 mL of medium was then added to 120 mL serum bottles, closed with a rubber stopper, and sealed. The medium was flushed with N_2/CO_2 the pH adjusted to pH 6.5 using HCl and the bottles were autoclaved (HV Series, Hirayama, Japan). After the bottles cooled down 0.2 mL of $Na_2S \cdot H_2O$ (0.61 mol L^{-1}) were added and the medium was flushed with H_2/CO_2. The medium was stored in the dark at room temperature.

Marine TE Solution

The marine TE solution contained 4 g NaBr, 1.8 g $SrCl_2 \cdot 6H_2O$, 0.529 g H_3BO_3, 1 g KI, 100 mg Na-silicate, 0.183 mg NaF, 100 mg KNO_3, 0.128 mg Na_2HPO_4 in 1 L of MQ water.

GenSkew

The location of the origin of replication for *M. smithii* was determined using GenSkew, which is a guanine/cytosine (GC) skew program developed by the University of Vienna that provides a graphical plot representing the GC skew and cumulative GC skew of the *M. smithii* chromosome using a genome from an existing database of genomes. GC and AT asymmetry result in divergent GC skew values and allows for the prediction of the origin and terminus regions. A minimum and maximum GC skew are calculated by utilizing windows of 1853 bp and the formula (G - C / G + C) to determine the difference of GC content in a window. The script then calculates for the entire genome in a stepwise manner, covering another 1853 bp and so on, until the entire genome has been analyzed. A GC skew curve and cumulative GC skew curve are generated in which the location of the oriC and terminus region can be visually observed, in addition to a calculated minimum and maximum.

Marker Frequency Analysis (MFA)

Marker frequency analysis (MFA) was used to support the GenSkew results for *M. smithii* and to be able to determine the oriC for *M. kandleri*. The gDNA was sequenced from an exponentially growing *M. smithii* and *M. kandleri* culture. An MFA was then run which maps the number of reads corresponding to each chromosome region. Given that the replication fork starts at the origin of replication, the number of reads should be the highest at the origin and lowest at the terminus of replication, allowing the determination of the oriC and ter on the *M. smithii* and *M. kandleri* chromosomes.

Direct-geneFISH

This protocol was adapted for use with *M. smithii* from Barrero-Canosa & Moraru (2021).

Primer design

Using the known location of the oriC and ter on the *M. smithii* genome from the GenSkew and MFA, Gene-PROBER developed by Dr. Cristina Moraru of the Moraru Phage Lab at the University of Oldenburg was used to generate FISH probes. For the ori probes, a 10,640 kb region of the genome was provided as a FASTA file into the program, to generate 11 forward and reverse primer sets for probes of each 300 bp in length; the region provided was slightly downstream of the predicted origin of replication. The same thing was done for the ter probes, but a 10,155 kb region of the genome was provided, and the probes were distributed upstream and downstream of the *XerA* gene. This program automatically checked for the possibility of primer dimer and hairpin formations and has been optimized already for DNA FISH by the Moraru Phage Lab.

Table 1 List of all ori primers used for DNA FISH. Primers ORI_3_FWD and ORI_3_REV were not used for DNA FISH due to amplification failure.

Primer Name	Sequence
ORI_1_FWD	TTCACTAATAGTCATGGCTC
ORI_1_REV	GAAGGAGAGGTAGACATGATTA
ORI_2_FWD	GATGTACTTGTTCACGAATCC

ORI_2_REV	GATTATTTGGGAGTTTGCCA
ORI_3_FWD	CCTATTACATCCAACACCATTC
ORI_3_REV	ATGTTCACTGCCTCTTCC
ORI_10_FWD	CTAGTTTAAACACCGGAATCAG
ORI_10_REV	CATCAATTGTTAAGCCACAGC
ORI_11_FWD	TAAACCAACTTACGGTGC
ORI_11_REV	CCAGCTTCAACTAATTTGTG
ORI_12_FWD	AATATGACGGAAGGGATTACG
ORI_12_REV	CCGGAATTCCTGCAAGATTA
ORI_13_FWD	CTTTGGAGAACTACCTACCC
ORI_13_REV	CTGCTTATGAGTGGTGAAAGAT
ORI_14_FWD	ATTCCATACACACACCTACG
ORI_14_REV	GAGTCGATTCCAACTTCCAT
ORI_17_FWD	GTATAATCTTCCTGAGTGTTGG
ORI_17_REV	GATGTCCTGTATGATGGGTATG
ORI_18_FWD	AGTGTAACCGCCTTTTGAG
ORI_18_REV	AAAAAGACATCCTCCAAGGT
ORI_19_FWD	ATATCTCCGGCCTATGTAC
ORI_19_REV	CTTCAGGTCATGCTAGTG

Table 2 List of all ter primers used for DNA FISH. Primers TER_1_FWD and TER_1_REV were not used for DNA FISH due to amplification failure.

Primer Name	**Sequence**
TER_1_FWD	CTTATTCCTCCAGTCAATCA
TER_1_REV	CCTAAAAAGGTCGGACATAA
TER_2_FWD	GCTAATGTTTGAGTCATGACC
TER_2_REV	TTCTGACATGTCTGTATGGG
TER_3_FWD	GTAATTCCATCCAGCTTAGACA
TER_3_REV	ATCGGAAGTGTGTATGCTTG
TER_4_FWD	TCTAGCACTGTCGCTAAAAT
TER_4_REV	ACCGATAAAGTAGGATGCAA
TER_10_FWD	GCCATTTAATCACCCGTTAT
TER_10_REV	TCTGACCAACTTTACTCTGC
TER_11_FWD	CTTTACCATCAATACGTCCT
TER_11_REV	TGAGAGATTTCGAACGTAC
TER_12_FWD	TAGCTTCTTCGTGAGTAATACC
TER_12_REV	GTATCGGTAAACCTATTGACG
TER_13_FWD	AACATACGACCCATCATATCTC
TER_13_REV	GCAGTGAGGCTTAAATATGA
TER_14_FWD	TTGTATTGTTTGACAGGTGG
TER_14_REV	AGATAAACGTCACTTCCCTTC
TER_15_FWD	AAGAGATGCATCTAAAGCCC
TER_15_REV	CAAGGTTACGATGTAGCACTTA
TER_16_FWD	GTCCATTAATGGGTTTCCAG
TER_16_REV	CTTCAAAAATGGCCTGTAAG

Primer testing and genomic DNA extraction

After designing the primers, the primers were ordered from Microsynth. Upon arrival, the primers were diluted from a concentration of 100 µmol L^{-1} to 10 µmol L^{-1} for use in PCR using DEPC H_2O. First, the *M. smithii* genomic DNA (gDNA) was extracted using a DNeasy PowerSoil Pro Kit (Qiagen, Germany) with a concentration between 25-200 ng

μL^{-1}. The amount used for PCR amplification of the probes was adjusted accordingly to get around 100 ng μL^{-1} of template per reaction. The DNA was eluted twice with 50 µL of DEPC water to obtain the purified gDNA.

Using gDNA and one forward and reverse primer—a probe set—11 probe sets were tested by attempting to amplify the 300 bp regions corresponding to the region for the origin of replication. Several primers were tested in parallel and under different conditions. A touchdown PCR program was used, where the annealing temperature reduced 0.3 °C every amplification cycle to target the ideal annealing temperature of the primers. A Taq polymerase (GoTaq DNA Polymerase, Promega, USA) was used for the PCR reactions. A master mix was used containing 5 µL of provided 5X GoTaq green buffer from Promega, 0.5 µL 10 mmol L^{-1} DNTPs, 0.5 µL of 10 µmol L^{-1} forward and reverse primer, 12.1 µL DEPC water, 0.15 µL of GoTaq polymerase, 0.25 µL of BSA, and 4 µL of *M. smithii* gDNA as a template, for a total reaction volume of 25 µL. The PCR was run using a Biometra TAdvanced Series thermocycler (Analytik Jena, Germany) at 95 °C for 5 min for initial denaturation and 72 °C for 10 min for final elongation, then left at 4 °C. 35 amplification cycles were performed at 95 °C for 30 s for denaturation, 57 or 58.5 °C start, depending on set of primers annealing temperature, with a 0.3 °C temperature drop each cycle for 30 s for annealing, and 72 °C for 30 s for elongation. A 1% agarose gel was run at 120 V using a Powerpac Basic (BIO-RAD, USA) for 40 min to check for successful fragment amplification.

Probe large batch amplification, PCR cleanup, and labeling

Large batch amplification and PCR cleanup

Large batches of the 300 bp probe fragments were amplified using the same PCR conditions as mentioned above, but for a total reaction volume of 50 µL with 8 replicates. Another 1% agarose gel was run at 120 V for 40 min using a Powerpac Basic (BIO-RAD, USA) to check successful fragment amplification. PCR cleanups of the big batches were performed using a Monarch PCR and DNA Cleanup Kit (New England Biolabs, USA). Each of the probe fragments were eluted in 6 µL of DEPC water and their concentrations measured with a N60/50 spectrophotometer (Implen, Germany) at 260 nm absorption. The probes were stored at -20 °C for later fluorescent labeling.

Labeling

For fluorescent labeling, the probes were diluted to 100 ng μL^{-1} with DEPC water, then 1 µL of each probe was combined for a total of 10 µL of FISH probe mix. The probe mix was then labeled with the Ulysis Alexa Fluor 594 ULS Nucleic Acid Labeling Kit (ThermoFisher Scientific, USA) following the manufacture's protocol. The probes were denatured for 5 min at 95 °C using a Biometra TAdvanced Series thermocycler (Analytik Jena, Germany), then 15 µL of fluorescent label was added. The mix was incubated for 30 min at 80 °C using a Biometra TAdvanced Series thermocycler (Analytik Jena, Germany) to label the DNA. The labeled probes were then purified, to separate unreacted ULS complex from the oligonucleotides, using a Micro Bio-Spin with Bio-Gel P-30 column (BIO-RAD, USA) following the manufacturer's protocol. Around 10 µL of the

probes were aliquoted into PCR tubes and stored away protected from light. To verify successful labeling and the quality of labeling, a NanoDrop 1000 spectrophotometer (ThermoFisher Scientific, USA) was used to specifically measure 594 nm wavelength absorption, which is the wavelength of the fluorescent tag. The device measured the number of fluorescent molecules to confirm successful labeling, and a generated spectrum indicated the quality. The labeling kit uses a universal linkage system which is based on the use of a platinum dye complex that forms a stable adduct with primarily N7 position guanines of our probes, resulting in the attachment of 594 nm wavelength fluorescent tags at these positions and consequently labeling of the probes.

Sample preparation

After labeling the probes, Direct-geneFISH was performed as originally described by Barrero-Canosa & Moraru (2021) with adaptations.

Slide and cell preparation

The samples were prepared on epoxy slides with eight 6 mm circular wells (Carl Roth, Germany) coated with 0.01% poly-L-lysine, enabling the attachment of cells to the slide. Fresh *M. smithii* cells were fixed from an exponentially growing culture at an OD 578 of around 0.3 using an ice-cold mixture of 80% methanol in 50 mmol L^{-1} Hepes pH 7. The cells were fixed in methanol for 10 min at -20 °C, then the cells were rehydrated in 400 µL of 50 mmol L^{-1} Hepes pH 7 for 10 min at room temperature. The cells were then permeabilized using 15 µL (15% v/v) of the phage endoisopeptidase from *Methanothermobacter wolfeii* (PEIW) with a concentration of 0.59 mg mL^{-1}, that was already shown to permeabilize *M. smithii* cells (Pende et al., 2021), in an 85 µL mixture of 50 mmol L^{-1} Hepes pH 7 with 1 mmol L^{-1} DTT, incubating for 10 min at 71 °C on a heat block shaking at 800 RPM (Smartblock, Eppendorf, Germany). The reaction was then stopped by placing it for 2 min on ice. After permeabilization, the cells were washed with 200 µL of 50 µmol L^{-1} Hepes pH 7 then washed by resuspending in 50 µL of 0.1% PBS-T (1X phosphate buffered saline with 0.1% Tween 20), sonicated in a water bath for 30 s, then 0.25 µL of cells were spread and dried in the wells on the epoxy slide (Carl Roth, Germany). PBS-T is specifically used to prevent cell aggregations that would make viewing under the microscope and cell detection during analysis more challenging, due to the addition of the gentle detergent Tween 20.

Hybridization and post hybridization

40 mL of hybridization buffer was prepared containing 8 g of dextran sulfate, 10 mL of 20X SSC (saline-sodium citrate), 1.6 mL of 0.5 mol L^{-1} EDTA pH 8, 16.4 mL of MQ water, 4 mL of 10% w/v nucleic acid blocking reagent (VectorLabs, USA), 1 mL of sheared salmon sperm DNA (ThermoFisher Scientific, USA), 1 mL of yeast RNA (ThermoFisher Scientific, USA), 200 µL of 20% w/v SDS, and 6 mL formamide (15% formamide final concentration). 600 pg μ^{L-1} of probes were mixed with hybridization buffer for a total of 40 µL. 30 µL of hybridization buffer was then pipetted on the surface of each well containing the cells. The slide was placed inside an airtight container with a wetted paper towel also containing 15% formamide—the same concentration used in the hybridization buffer—on a small plastic rack and then hybridization was carried out for

40 min at 85 °C and then samples were incubated overnight at 46 °C in a convection drying oven (BOF-200 Forced-air Drying Oven, Being Lab, USA). The next day the cells were washed at 48 °C in a water bath for 15 min with a washing solution containing 500 µL of 0.5 mol L^{-1} EDTA pH 8, 700 µL of 5 mol L^{-1} NaCl, 1 mL of 1 mol L^{-1} Tris-HCl, 25 µL of 20% SDS w/v, and 47.8 mL of MQ water. The cells went through a final wash with 1X PBS for 10 min then were completely dried.

Hoechst staining and embedding

The cells were stained with a 1:2000 Hoechst 33258 DNA stain (ThermoFisher Scientific, USA) in 50 mmol L^{-1} Hepes pH 7 and incubated for 10 min, then a final wash was performed with 1X PBS and MQ water for 1 min each. The slide was completely dried then 2 µL of VectaShield (VectorLabs, USA) mounting medium was added to each well containing the stained cells, a 24 x 50 mm glass coverslip (Carl Roth, Germany) was placed on top of the slide and the coverslip edges were sealed with generic nail polish.

Microscopy and image analysis

The slide of the Direct-geneFISH experiment was examined under an epifluorescence microscope (Eclipse NI-L, Nikon, Japan), with a 100X objective and an Alexa 594 and DAPI filter. Images were taken with an exposure time of 10 ms for phase contrast images, 2000 ms for Alexa 594 images, and 20 ms for Hoechst images. A set of three images (phase, Alexa 594, and Hoechst), for a total of 10 images, were taken and made into hyperstacks. Image analysis was done in Fiji using the plugin MicrobeJ (Ducret et al., 2016). The cell outlines were traced and the cell length, width, fluorescence intensity along the cell length, and presence of fluorescent maxima were measured automatically. Automatically recognized cells were manually double-checked. For the plots showing the relative position of detected maxima, cells were automatically grouped into two classes according to the detected fluorescent maxima (non-dividing and dividing). The relative position of detected maxima plots was created in MicrobeJ, representative cells were chosen from larger fields of view, and their brightness and contrast were adapted in Fiji. This analysis was used to support observations made from the representative image in *M. smithii*.

RASER-FISH

Sample Preparation

The same sample preparation protocol, up to post-permeabilization, and microscopy and image analysis were used from Direct-geneFISH for RASER-FISH. This protocol was adapted for use with *M. smithii* from Brown et al (2022). and Barrero-Canosa & Moraru (2021).

Slide and cell preparation

Fresh *M. smithii* cells were taken from an exponentially growing culture at an OD 578 of around 0.35. After permeabilization, the cells were washed for 2 min with 200 µL of 50 mmol L^{-1} Hepes pH 7, then washed for another 2 min in 200 µL of 0.1% PBS-T (1X

phosphate buffered saline with 0.1% Tween 20). The cells were then quickly resuspended in 50 µL of 0.05% Triton X-100 in 50 mmol L^{-1} Hepes pH 7, transferred to a 200 µL PCR tube, sonicated in a sonication water bath for 30 s, then 0.25 µL of cells were spread and dried in a well on the epoxy slide —PBS-T and Triton X-100 are specifically used to prevent cell aggregations that would make viewing under the microscope and cell detection during analysis more challenging, due to the addition of the gentle detergent Tween 20 and harsher detergent Triton X-100. The cells were then washed for 1 min with MQW then absolute ethanol.

Pre-hybridization

30 µL of exonuclease III solution (1.5 µL 100 U $µL^{-1}$ exonuclease III from *E. coli* (New England Biolabs, USA), 3 µL kit-provided buffer (New England Biolabs, USA), and 25.5 µL DEPC H_2O) was pipetted on top of the cells in the well. The slide was placed into a waterproof container and floated in a water bath (1235PC Digital Water Bath, VWR, USA) at 37 °C for 10 min. The slide was then washed for 2 min in 1X PBS, at room temperature, three times, the finally washed for 1 min in MQW at room temperature. The slide was dried completely for the hybridization step.

Hybridization and post hybridization

30 µL of hybridization buffer, also used for Direct-geneFISH, was pipetted on top of the cells in the well. 600 pg $µL^{-1}$ of probes were mixed with hybridization buffer. The slide was placed into a waterproof container and floated in a water bath (1235PC Digital Water Bath, VWR, USA) at 38 °C overnight (approximately 15 h). The next day the cells were washed 2 times in 2X SSC for 10 min at 37 °C in a water bath (1235PC Digital Water Bath, VWR, USA), then washed once at room temperature in 2X SSC. The cells went through a final wash with 1X PBS for 1 min then with MQW. Finally, the slide was completely dried for the next step.

Hoechst staining and embedding

The cells were stained with a 1:2000 Hoechst 33258 DNA stain (ThermoFisher Scientific, USA) in 50 mmol L^{-1} Hepes pH 7 and incubated for 10 min, then a final wash was performed with 1X PBS and MQ water for 1 min each. The slide was completely dried then 2 µL of VectaShield (VectorLabs, USA) mounting medium was added to the well containing, a 24 x 50 mm glass coverslip (Carl Roth, Germany) was placed on top of the slide and the coverslip edges were sealed with nail polish.

qPCR of *M. smithii* and *M. kandleri*

Standard design and preparation

Primer design

The primers were designed on Primer3Plus (https://www.primer3plus.com/) using the “general settings” in Figure 7 and default settings for everything else. The primers were ordered from Microsynth.

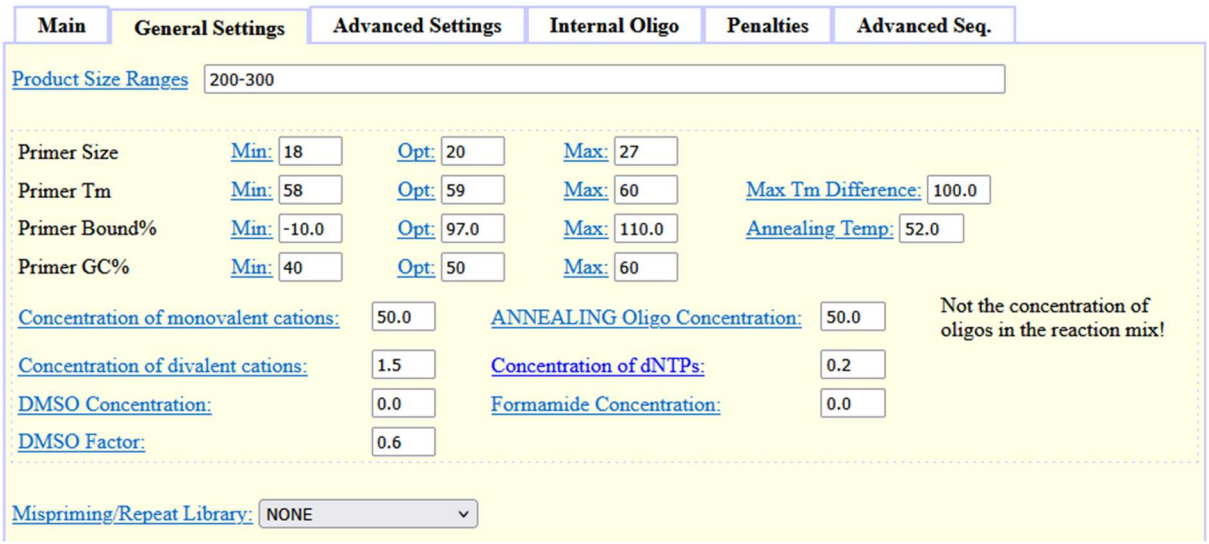

Figure 7 The modified parameters used in Primer3Plus.

The designed primers are shown in Table 3. These primers were designed to amplify a 207 bp region for part of the *cdc6* gene of *M. smithii* and 224 bp region for part of the *ftsa* gene of *M. kandleri*. These were designed around the oriC of each species to make sure it would be present in all cells during qPCR to obtain the most accurate results.

Table 3 List of all primers used for amplification of qPCR fragments

Primer Name	Sequence
MS_CDC6_FWD	TGTAATGCAATTTTTAGCGGGAAGC
MS_CDC6_REV	AGCTCTGCGAAGGTTCTGTAGG
MK_FTSA_FWD	TCGTCCGTGCTGTCTACACC
MK_FTSA_REV	ATCGATGAGTTCCGAGCCCC

Table 4 Complete list of gene sequences used for generating the primers.

Gene Name	Sequence
Ms *cdc6*	5’ ATGTTCACCATTTTAAAAAGTAATAAAAAAATAATCTTAAAAACATGAAAAAATCATAAGTATTATTTCC AGTGATAATATATGAAAACAGTGTTAAATAAAGGTTTGTATTACAAAATTGTATTGAAATAATAAATTTTA TTATAAAATAAAAAATAAAAACATTTAAATAAATTAAAATTAACTAAAAAATGTTTAAAATAATTTAATCTA TAAAAAACAAATAATTAATAGATTAAATAAAAATTAAAGTGAATATGATTAGTTAAAATTAAAACATGAA AAATAACTATTTCAAATATAAAGACATATATTTCAAGTGAAAAAAGAGTAATAAAAATAGAATTAATATA ATCATAAAATAAATTTACAATTTTTAAATTATAAAATAAAAACAGCAAATTAAATATTTTTAAAAAATAAG AAGTTTAAAACAATTTTTTATAAAATAAATTATTTTAAAAATTTTTTAAAAAAATAAAAACAATAAAAATAA AGCTAAAACAATTTTTATTTCAAAATTAAAGAAGATAAATTTCAATTGTAATAATTTCAGTTAAATATAAT ATTTATCTGAGCATTTGAAAAATAAAACATATATTTCAAGTGAAAAAAAATCTGAAAAAGGATTTAATA AAAAAATTTATAATGATTTATCATAAAAAGTGAGAGATAAATTTCAAGTGTAATGCAATTTTTAGCGGG AAGCAAAAATCAAGACATTGATTTCAAGTGAAAAAAAATTTTAAAATGAATTAAAAAAGTTATTTCAGT AAAAAAAGAATGGAAAATGTTTTATTTTAAATTTAAACCAAGAAAAATTAAGATAAATTTCAAGTGTTTT TACAGATGAAATACATGTCTTCATTCCTACAGAACCTTCGCAGAGCTTTCACTTGAAATTCATGTCT GTCTGTCTGTCTAAAATTTATAAAAAAA 3’
Mk *ftsa*	5’ TTAACGAGGCTCATTACCTCCGGAATCGTCCAGCCCCTCCTTAAGACCAGTAACGTTGCCCGC CGTCTCACTTACTCCACCCTCGACCTCTTGGAGTTCGTCTACCGGGATGAGGATGGGCCCCAT

	CTCCTTAACTTGGACTATTTTGTACTCCTTCGGGAGCGTGTCCACGGTATCTTCCACTTCCGACC CACTGACGTTCACCTTAACGCCATCGACGTCGTCCGTGCTGTCTACACCCTCGAACTTGATAGTT ACCGTACCAGCGTACGCCCGGCCACGGAGTTCCGCTGTTACGGGCGCTGGTTGCATCAGGAT TATCTCCTTAATGGCACTAATGATGGCTTCCTTCAGCCCCGTCCTCCTCGGGATCTTTACGGAATC TTCGATCCGGCCCCCTACTTCGAGGTAATACCGACCTTCGGGGGCTCGGAACTCATCGATGAC CACTTTCACATCACGACCGGAGCACTGCTGACATAGGGCGGTATCGCGGAGTACGGAGACCG CCACCACACGCATGGGTCCCGCGAGTTGCTTTCCGATGTGTGGTATCTTCGAAGCTTCGAGCAT CTCCACTCTGGGTACTATCCCTAGGTAATCACGATAGGCATCAAGAATAGCTTCCCGAACGGCC GTTTCAGCCTGATCGAGCAAGACTCCGCCTCCGTACAACTCGACCCGCTCCGGGACGTTCATG TCTAAGCTCCTGATGATACTCTTAACGGCCGACCTCACGGCGTCCCGGACGTACTCCGCGACC TCTTCGATGGCCTCCAACACCTCACGGCGGGTAAGGTCGTACCGTGAGAGTTCCGAATCGGCC ATCGGCGAATTGATCTTCTTTTTGATATTTTCCGCTTCTTCATATGTTAGTCCTAAATCATTAGCTATG GCTAAGGTAAAATCACGTCCGCCAACTTTAATAGAATGACACACTTCCACAAGTGTGTTACGCAC AACGGAGATATCCGTAGTACCTCCACCGGAATCAATTAGGAGGCAGTTCTCGATTTTGTAATCTCT GATCGCTTTGGCCACGGCGAGGGGTTCAACCGATATCGTGATTAACTTCATATTAAGGAGCCTAG CGATGCGCTCTAGGTTATTAATGAGCCCCAAGCTTGTATTCGATACTATGGCCCTGAACTGCAAGT GAGTGACTTGAGAACCGATGAGACCGTCGGGGTGGTCTGCCCCGAGTTCCCTTGGGTCTACCT CTGCTCCGTCGACCTTGAGATCCACTATATCGACGGAGATAGGCCAGTTTTCGGGCGAGAACTC CAAGCGGTGCGCTAGCGTGTATCCTATGTCCTCTATGCGGAGCTTTCCTTCGGGGCTCACGCTC GCCTCCGCTTCCACCATAGTGAACCGGTCTCCCGTCATCGACAATCCGATACCCTCTACGTCC GAAGGACTGACCCCTGCATCACGAAGTGCTTCTTCTACGGTTTTCTTGACTATCCGGCTCACACC CTTCACGTATCTGACGTTTCCTCGCTCCATGATCGTGGGATCGAGGATGTACCGCTCGCTGTACC CCTTGACCATCAGGTTACCACTCCTGAGTCGCCCTACGGCGGCTGAGATCACCTCGGTACCCA AGTCTACGGCGACCAC 3’
Ms qPCR Frag	5’ TGTAATGCAATTTTTAGCGGGAAGCAAAAATCAAGACATTGATTTCAAGTGAAAAAAAATTTTAAAAT GAATTAAAAAAGTTATTTCAGTAAAAAAAGAATGGAAAATGTTTTATTTTAAATTTAAACCAAGAAAAA TTAAGATAAATTTCAAGTGTTTTTACAGATGAAATACATGTCTTCATTCCTACAGAACCTTCGCAGAG CT 3’
Mk qPCR Frag	5’ TCGTCCGTGCTGTCTACACCCTCGAACTTGATAGTTACCGTACCAGCGTACGCCCGGCCACGG AGTTCCGCTGTTACGGGCGCTGGTTGCATCAGGATTATCTCCTTAATGGCACTAATGATGGCTTC CTTCAGCCCCGTCCTCCTCGGGATCTTTACGGAATCTTCGATCCGGCCCCCTACTTCGAGGTAA TACCGACCTTCGGGGGCTCGGAACTCATCGAT 3’

PCR and cleanup

The primers arrived as powder and were diluted with DEPC H_2O to a concentration of 100 µmol L^{-1}. The primers were further diluted to 10 µmol L^{-1} for use in PCR using DEPC H_2O. *M. smithii* genomic DNA (gDNA) was extracted using phenol-chloroform extraction. A concentration of 370.6 ng $µL^{-1}$ for *M. smithii* and 43.65 ng $µL^{-1}$ for *M. kandleri* was obtained. For use in PCR amplification, the *M. smithii* gDNA was diluted 1:100 to around 3.7 ng $µL^{-1}$ and the *M. kandleri* 1:10 to around 4 ng $µL^{-1}$.

Using gDNA and the primer set for either the *M. smithii cdc6* gene or *M. kandleri ftsa* gene, the around 200 bp fragments were amplified by PCR. A Taq polymerase (GoTaq DNA Polymerase, Promega, USA) was used for the reactions. A master mix was used containing 5 µL of provided 5X GoTaq green buffer from Promega, 0.5 µL 10 mmol L^{-1} DNTPs, 0.5 µL of 10 µmol L^{-1} forward and reverse primer, 15.1 µL DEPC water, 0.15 µL of GoTaq polymerase, 0.25 µL of BSA, and 1 µL of *M. smithii* or *M. kandleri* diluted gDNA as a template, for a total reaction volume of 25 µL. The PCR was run using a Biometra TAdvanced Series thermocycler (Analytik Jena, Germany) at 95 °C for 5 min for initial denaturation and 72 °C for 10 min for final elongation, then left at 4 °C. 35 amplification

cycles were performed at 94 °C for 30 s for denaturation, 55 °C for 30 s for annealing, and 72 °C for 40 s for elongation. A 1% agarose gel was run at 120 V for 40 min using a Powerpac Basic (BIO-RAD, USA) to check for successful fragment amplification. The PCR products were then purified using a Monarch PCR & DNA Cleanup Kit (New England Biolabs, USA) and their final concentrations measured with a N60/50 spectrophotometer (Implen, Germany) at 260 nm absorption.

Cloning

A CloneJET PCR Cloning Kit (ThermoFisher Scientific, USA) was used to clone the short gene fragments of *M. smithii cdc6* and *M. kandleri ftsA* into a pjet 1.2 plasmid. The manufacturers protocol was used except that a ratio was not calculated for cloning, rather just 1 µL of the fragments were added to the reaction.

Transformation

E. coli TOP10 cells were transformed with either the *M. smithii cdc6* and *M. kandleri ftsa* gene fragments. 30 µL of frozen TOP10 cells were thawed on ice and 3 µL of the gene fragment was added. The cells were incubated on ice for 30 min, followed by a heat shock at 42 °C for 30 s on a heat block (Smartblock, Eppendorf, Germany). The cells were incubated again on ice for 5 min then 200 µL of SOC (super optimal broth with catabolite inhibition) medium was added for recovery. The cells were shaken at 37 °C, 400 RPM on a heat block (Smartblock, Eppendorf, Germany), for 40 min. Thereafter, the cells were plated onto 0.1% ampicillin (100 µg mL^{-1}) LB agar plates and incubated overnight at 37 °C (Incubator BD Series, Carl Roth, Germany). Work was done under a flame when adding SOC and during plating.

Colony PCR

For the colony PCR, A Taq polymerase (GoTaq DNA Polymerase, Promega, USA) was used. Each PCR reaction consisted of 5 µL of 5X GoTaq Green buffer, 0.5 µL of 10 mmol L^{-1} dNTPs, 0.5 µL of 10 mmol L^{-1} pjet 1.2 forward and reverse primers, 16.875 µL of DEPC water, 0.125 µL of DNA polymerase, 1.5 µL of 7.5 mmol L^{-1} $MgCl_2$, and a colony picked with a pipette tip, resulting in a total reaction volume of 25 µL. To prepare the colony template, a sterile pipette tip was used to scrape a colony from the agar plate under flame. The colony was then immediately transferred and stirred into a PCR tube already containing the reaction mixture. This process was repeated for all colonies. Additionally, a master plate was created by briefly touching a small section of the plate with the pipette tip from the PCR tube before disposing it.

The PCR was run using a Biometra TAdvanced Series thermocycler (Analytik Jena, Germany) and the conditions were as follows: initial denaturation at 95 °C for 3 min, followed by 25 cycles of 30 s at 94 °C (denaturation), 30 s at 60 °C (annealing), and 40 s at 72 °C (elongation), with a final elongation step at 72 °C for 5 min. To verify successful amplification, a 1% agarose gel was run in 1X TBE buffer at 120 V for 40 min using a Powerpac Basic (BIO-RAD, USA).

Sequencing

Using provided pjet 1.2 forward and reverse primers, the successfully transformed plasmids were sent for sequencing to confirm the insert was in the correct direction in the plasmid and that transformation was successful.

Plasmid production and purification

The best colony from sequencing that successfully was cloned and transformed was grown in 5 mL LB and 5 µL (1:1000) ampicillin (100 µg mL^{-1}) at 37 °C shaking at 400 RPM on a heat block (Smartblock, Eppendorf, Germany). The plasmids were then purified using the Monarch Plasmid Miniprep Kit (New England Biolabs, USA) following the manufacturer's protocol and then stored at -20 °C.

Plasmid linearization

Each of the plasmids were linearized for use in qPCR. 1 µg of either gene fragment (2.1 µL *M. smithii cdc6* and 3.3 µL *M. kandleri ftsa*), 5 µL 10X CutSmart buffer (New England Biolabs, USA), 1 µL of Hind III-HF enzyme (New England Biolabs, USA), and DEPC H_2O to the final volume (41.9 µL *M. smithii cdc6* and 40.7 µL *M. kandleri ftsa*) was added to a 1.5 mL Eppendorf tube. The reaction was incubated in a heat block for 1 h at 37 °C (Smartblock, Eppendorf, Germany). The tube was then placed at 80 °C for 30 min to heat-inactivate the enzyme (Smartblock, Eppendorf, Germany). The linearized plasmid was stored at -20 °C.

qPCR

Cell counting

1 mL of culture was added to three 1.5 mL Eppendorf tubes then each was diluted 1:10 in MQW. Cell counts were performed in triplicates with each tube acting as a replicate. A 0.01 mm depth 0.0025 mm^2 Neubauer Improved Counting Chamber (hemocytometer) (Paul Marienfeld, Germany) was used for cell counting under phase contrast with an Eclipse NI-L microscope (Nikon, Japan). Before adding the cells to the counting chamber, the cells were vortexed for 5 s to ensure homogenous distribution of cells. The cells were counted in a Z pattern using the central 5x5 grid, skipping every other square, to count a total of 13 inner squares in the chamber. Zooming in/out was done to check for cells at different viewing planes. The formula shown in $\left(\frac{T}{N \cdot S^2 \cdot D}\right) \cdot C$

Figure 8 was used to calculate the final cell count μL^{-1}.

$$\left(\frac{T}{N \cdot S^2 \cdot D}\right) \cdot C$$

Figure 8 Formula for calculating final cell count μL^{-1}. T = total number of cells counted, N = number of squares counted out of 25 (5x5 grid), S = square size in mm, D = chamber depth in mm, and C = cell dilution.

DNA extraction

Phenol-chloroform extraction was performed using an adapted protocol originally from Basile Beaud. A lysis buffer was made containing 1 mL of 10% SDS, 200 µL 5 mol L^{-1} NaCl, 100 µL 1 mol L^{-1} pH = 8 TrisHCl, 20 µL 0.5 mol L^{-1} EDTA, and filled to 10 mL with MQW. DNA was extracted by first centrifuging 1 mL of culture (adjusted for density) at 16,000 RCF for 2 min (MiniSpin, Eppendorf, Germany). The supernatant was discarded, and the pellet was resuspended in 100 µL of lysis buffer. The resuspension was transferred into a FastPrep tube containing 100 µL of 0.2–0.5 mm glass beads (Lysing Matrix E, MP Bio, USA). A volume of 100 µL phenol/chloroform was then added using a 1 mL glass pipette. The mixture was bead beaten with a bead beater four times at 6 m/s for 30 s, with a 60-s rest between cycles (FastPrep-24, MP Bio, USA). Following lysis, 200 µL of 1X SSC was added, the sample was vortexed for 5 s and then centrifuged at 16,000 RCF for 3 min (Centrifuge 5425, Eppendorf, Germany). The top aqueous phase was transferred to a fresh 1.5 mL Eppendorf tube, followed by the addition of 200 µL phenol/chloroform, and centrifuged again at 16,000 RCF for 3 min (Centrifuge 5425, Eppendorf, Germany). Approximately 180 µL of the upper phase was transferred to a new tube, and 400 µL of cold 100% ethanol was added. The sample was incubated on ice for 10 minutes, then centrifuged at 16,000 RCF for 1 min (Centrifuge 5425, Eppendorf, Germany). The supernatant was discarded, and the pellet was gently resuspended in 1 mL of 70% ethanol. The sample was centrifuged (Centrifuge 5425, Eppendorf, Germany) at 16,000 RCF for 5 min at 4 °C. The supernatant was removed, and the pellet was dried by inverting the tube onto a paper towel, followed by air drying. The pellet was resuspended in 30 µL of DEPC-treated water and incubated at 42 °C for 10 min. DNA concentration was measured with a N60/50 spectrophotometer (Implen, Germany) at 260 nm absorption. The gDNA was stored at –20 °C.

qPCR

Qubit

A Qubit 2.0 fluorometer (ThermoFisher Scientific, USA), using the broad range buffer and manufacturer's protocol, was used to accurately measure the concentration in ng μL^{-1} of the linearized plasmid for each gene fragment. Precise measurement is required, since this plasmid acts as the standard in the qPCR and will act as a reference for all the data.

Copy number calculation

After obtaining the concentration, the copy number was calculated, as this is an input for the qPCR machine and reference for the data. The copy number was calculated using the formula in **Figure 9**. For the *M. smithii cdc6* plasmid a length of 3181 bp was used and for the *M. kandleri ftsa* plasmid length a length of 3198 bp was used.

$$\text{Copy Number} = \left(\frac{\text{Amount of DNA (ng)} \times 6.022 \times 10^{23}}{\text{Molecular Weight (g/mol)} \times 10^{9}} \right)$$

$$\text{Molecular Weight} = 660 \text{ g mol}^{-1}\text{bp}^{-1} \cdot \text{length of plasmid (bp)}$$

Figure 9 Formula used for calculating copy number.

Sample preparation and loading

The standards for each plasmid were diluted with DEPC H_2O in 1.5 mL Eppendorf tubes. 18 µL of DEPC H_2O and 2 µL of the 10^8 standard was added then this was repeated in this order: 10^8->10^7->10^6->10^5->10^4->10^3->10^2->10^1. Each time, the Eppendorf was vortexed for 10 s and spun for 10 s, before pipetting the next dilution. The gDNA extracted earlier was also diluted 1:10 and 1:100.

A 2X Luna Universal qPCR Master Mix (New England Biolabs, USA) was used. Each reaction had 10 µL of 2X Luna mix, 0.5 µL of forward and reverse primer, 4 µL DEPC water, and 5 µL of either standard or gDNA for a final volume of 20 µL. This was prepared in qPCR tube strips (BIO-RAD, USA). The qPCR was loaded as shown in **Error! Reference source not found.**. The qPCR was run with a CFX Connect qPCR machine (BIO-RAD, USA).

Data analysis

The data was used to determine the ploidy using the formula in Figure 10.

$$\text{Ploidy} = \frac{\text{Cell count}}{\text{SQ (copy num.)}}$$

Figure 10 Formula for calculating ploidy. Cell count is the average cell count of the triplicate counts and SQ is the value given by the qPCR machine that correlates to copy number.

It was checked that the Cq/Ct values and SQ values of the triplicates did not have large differences between them. It was also checked that the Cq/Ct values of the standards had only a difference of 3-4, indicating an exponential standard curve.

Results

M. smithii results

OriC and ter determined using GenSkew and MFA

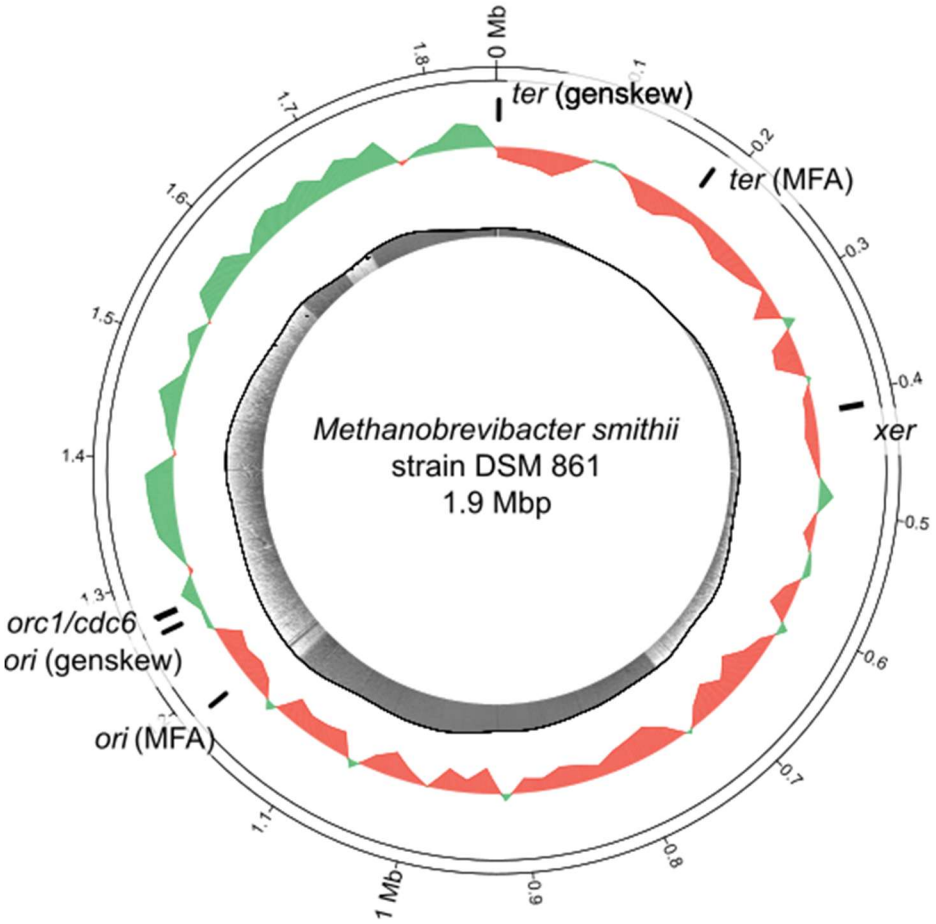

Figure 11 Genome map of *M. smithii* with GenSkew and MFA results. The GC skew values based on the GenSkew analysis (green/red), and the marker frequency analysis (MFA) results (gray) are mapped on the *M. smithii* genome. The genes associated with oriC (*orc1/cdc6*) and the ter (*xer*A) are also shown for reference. The outer ring displays the genome size in Megabases (Mb), the central ring displays the GenSkew analysis (with green indicating the GC skew of the leading and red the GC skew of the lagging strand) and the inner ring displays the results of the MFA. Image and analysis by Tobias Viehboeck.

We used two in-silico approaches to predict the position of the oriC and ter: 1) GenSkew, which is a program that measures the GC content by reading the genome sequence by frames (short sections of the genome) and calculating whether it is positively or negatively biased (GC skew). Since the program automatically identified where there were inversions in the GC content, we could estimate the location of the oriC and ter as a minimum and maximum GC skew, respectively; 2) marker frequency analysis (MFA) which uses sequencing of DNA from an exponentially growing culture

and a script to quantify the number of adenosine (A) and thymine (T) nucleotide reads. These results are mapped and provided as a graph. The oriC contains a higher number of AT during DNA replication, allowing for approximation of the oriC location in the genome and consequently the ter, which is opposite of the oriC, using MFA. The GenSkew analysis suggested the oriC at around 1.26 Mb and the terminus of replication (ter) at around 0 Mb (Figure 11). We can observe this by the GC skew inversions, which are where the red and green graphs meet. The MFA results indicate the oriC to be at around 1.19 Mb and the ter at around 0.19 Mb. We can observe this in the graph with the read number, highest at and near the oriC and lowest at the ter. With only one oriC and ter found using GenSkew and MFA, we concluded that there is only one oriC for each chromosome of *M. smithii*.

DNA staining indicates monoploidy

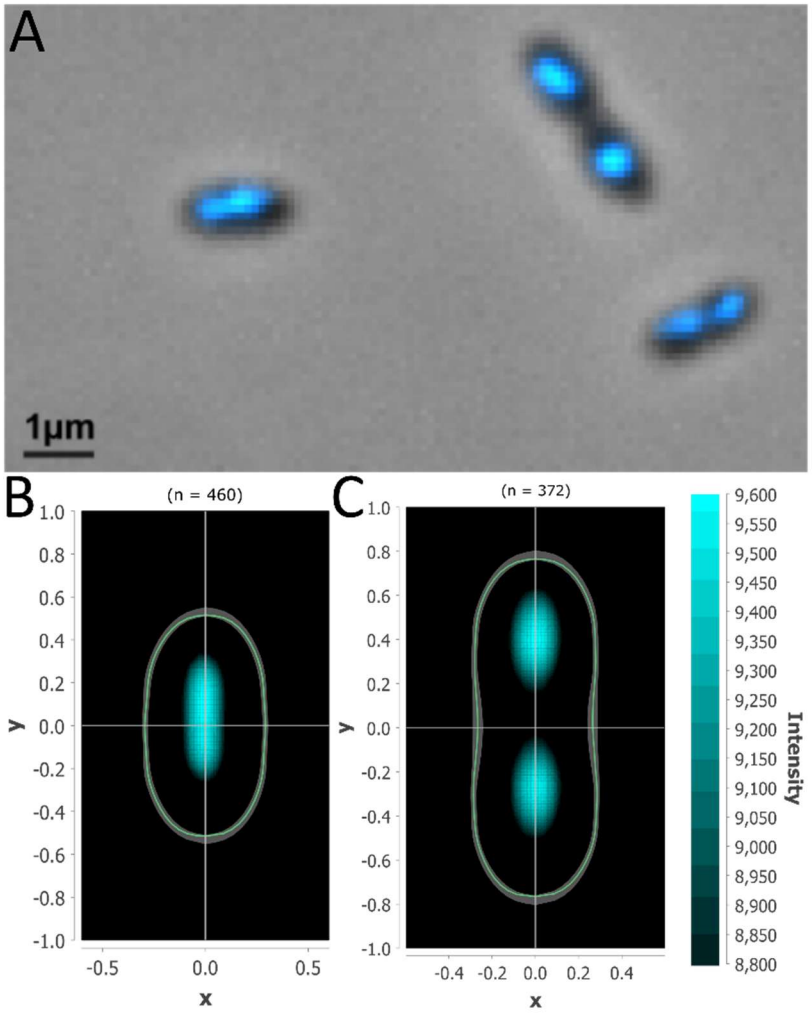

Figure 12 DNA staining with Hoechst representative image and quantitative analysis of fluorescent maxima in *M. smithii*. The x and y axes show the relative position of fluorescent foci within the cell. The intensity indicates the brightness of the foci in a certain location with bright cyan (0.9) being the highest. The cell outline represents the mean cell outline from all the cell corresponding to one plot. (B) shows

the focus of non-dividing cells and (C) shows the foci of dividing cells. (n) indicates the cell number in which the fluorescent maxima were detected. Representative image made by Nika Pende.

We stained the DNA with Hoechst stain. In the representative image, the DNA appears as a single focus in non-dividing cells and as two foci in dividing cells (Figure 12A). DNA signal is centrally localized as a single focus in non-dividing (Figure 12B; n = 460) and as two foci in dividing cells, one per daughter cell (Figure 12C; n = 372).

DNA Direct-geneFISH and RASER-FISH targeting the oriC reveal monoploidy and longitudinal chromosome configuration

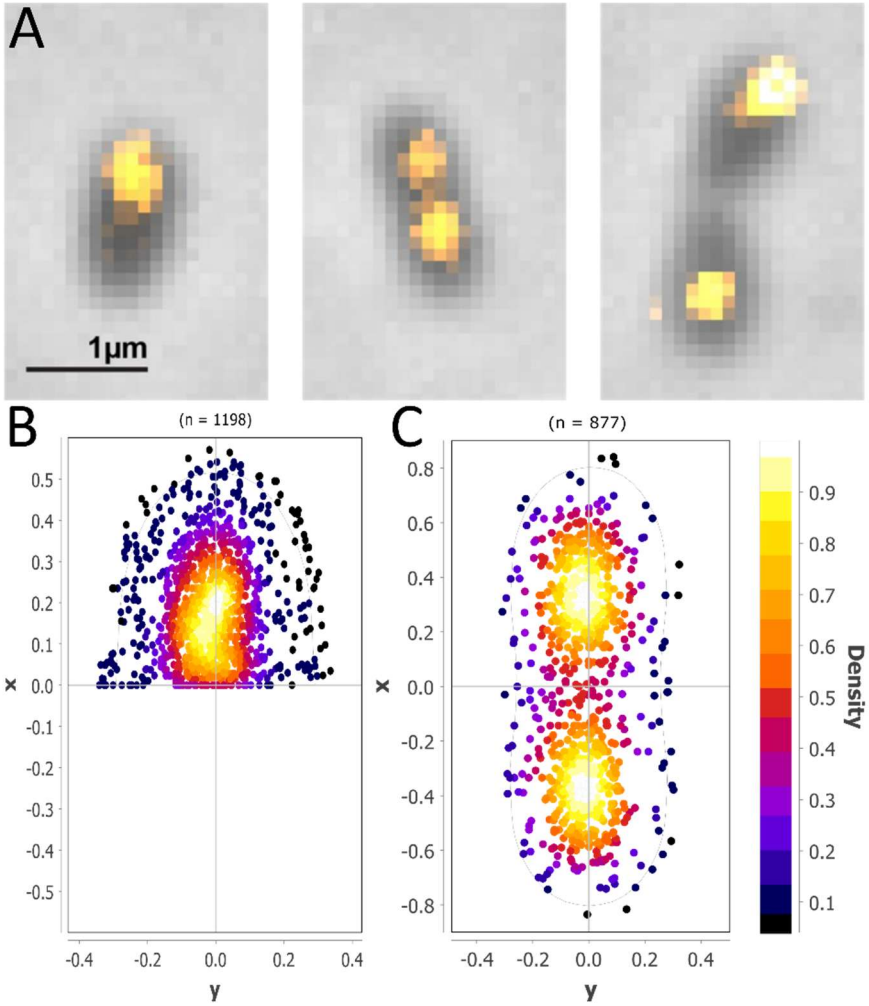

Figure 13 Direct-geneFISH representative image and quantitative analysis of fluorescent maxima of the oriC in *M. smithii*. (A) phase contrast images with a fluorescent overlay of the origin of replication labeled with Alexa 594 (orange). (B) shows a non-dividing cell, center panel shows a cell constricting, and (C) shows a dividing cell completing division. (Bottom) quantitative analysis plots where the x and y axes show the relative position of fluorescent foci within a cell. The more yellow/white, the higher the number of foci in a certain location, with white (1.0) being the highest density of foci.

The cell outline represents the mean cell outline from all the cells. (B) are the foci of non-dividing cells and (C) are the foci of dividing cells. (n) indicates the cell number in which the fluorescent maxima were detected. Representative image by Nika Pende.

In the representative image, we can observe that in non-dividing cells, there is only one fluorescent focus corresponding to one origin of replication (Figure 13A, left). In constricting (Figure 13A, center) and cells concluding division (Figure 13A, right), we can see that there are two fluorescence foci, one per daughter cell. For the quantification, we separated the data into two classes: 1) cells that are non-dividing and 2) cells that are dividing. Based on the analysis, non-dividing cells have one fluorescence focus (Figure 13B) while dividing cells have two foci (Figure 13C). More precisely, in non-dividing cells, the focus is localized at one third (subpolar; the center of the cell (mid-cell) corresponds to 0 on the x-axis and y-axis). In dividing cells, the foci appear to be localized at the mid-cell of each prospective daughter cell. The splitting of one focus to two foci also indicates that the chromosomes are segregated along the long axis of the cell.

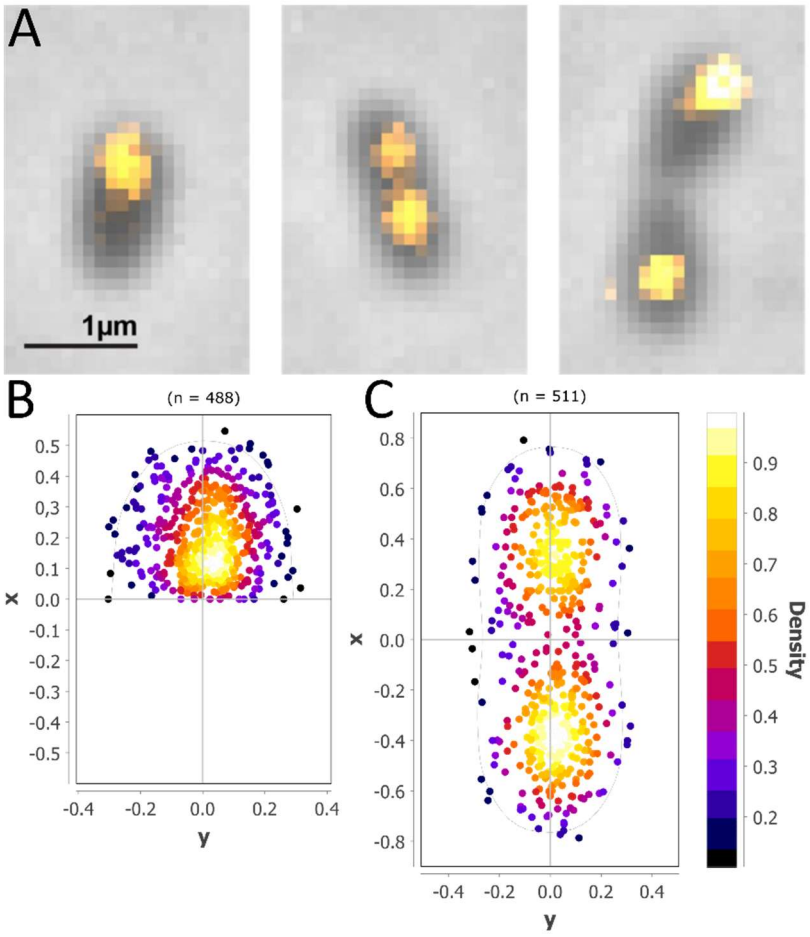

Figure 14 RASER-FISH quantitative analysis of fluorescent maxima of the oriC in *M. smithii*. The x and y axes show the relative position of fluorescent foci within a cell. The more yellow/white, the higher the number of foci in a certain location, with white (1.0) being the highest density of foci. The cell outline represents the mean cell outline from

all the cells. In (B) are the foci of non-dividing cells and in (C) are the foci of dividing cells. (n) indicates the cell number in which the fluorescent maxima were detected. Representative image by Nika Pende.

The representative image for the ori looked the same for both Direct-geneFISH and RASER-FISH (Figure 14A). We performed the same quantitative analysis using RASER-FISH-based images. We observe that the RASER-FISH-detected foci in non-dividing cells appear more mid-cell than Direct-geneFISH-detected foci (Figure 13B, Figure 14B). The foci in the RASER-FISH quantitative analysis plot also appear to be more tightly clustered towards the highest density than in the quantitative analysis plot of the Direct-geneFISH results. All in all, we concluded that *M. smithii* is monoploid and that its chromosome is longitudinally configured.

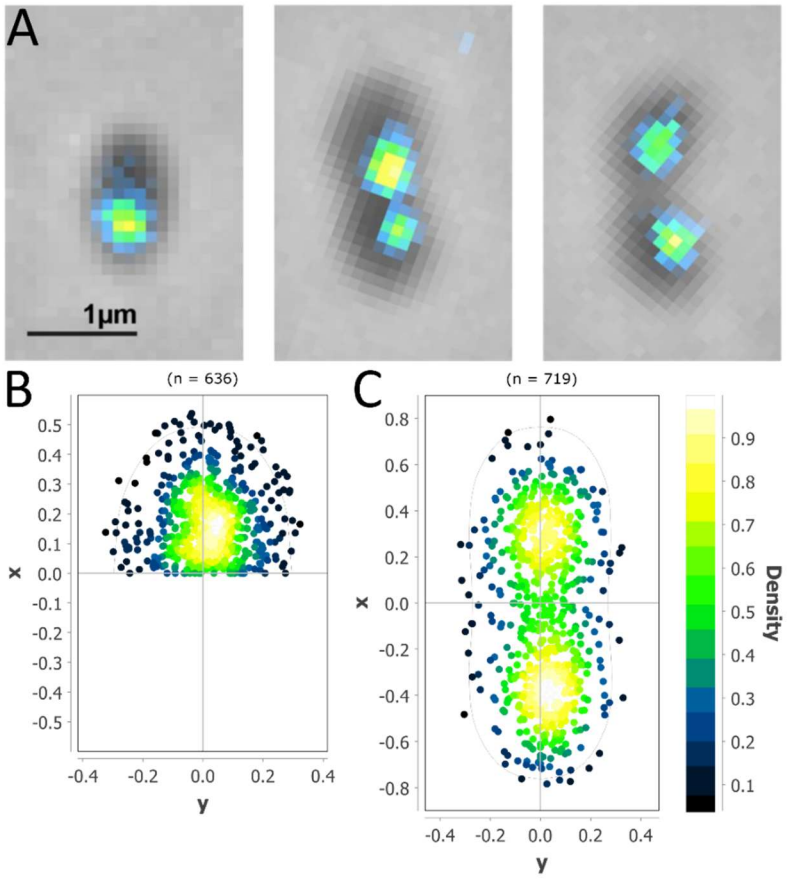

Figure 15 Direct-geneFISH representative image and quantitative analysis of fluorescent maxima of the *xera* region in *M. smithii*. (Top) phase contrast image with a fluorescent overlay of the origin of replication labeled with Alexa 594 (orange). (A) left shows a non-dividing cell, center shows a cell constricting and right shows a dividing cell completing division. B & C show the quantitative analysis plots where the x and y axes show the relative position of fluorescent foci within a cell. The more yellow/white, the higher the number of foci in a certain location, with white (1.0) being the highest density of foci. The cell outline represents the mean cell outline from all the cells. In (B)

are the foci of non-dividing cells and in (C) are the foci of dividing cells. (n) indicates the cell number in which the fluorescent maxima were detected. Representative image by Nika Pende.

For the ter representative image, we can observe that in non-dividing cells (Figure 15A, left), there is only one fluorescent focus. In constricting (Figure 15A, center) and cells concluding division (Figure 15A, right), we can see that there are two fluorescent foci. Collectively, we concluded that *M. smithii* is monoploid. Based on the quantitative analysis of the ter, we observe that non-dividing cells have one focus (Figure 15B) while dividing cells have two foci (Figure 15C). The foci polarization away from the mid-cell that we observe in the representative image, specifically for constricting cells (Figure 15A, center), is not seen in the quantitative analysis of non-dividing cells (Figure 15C). The ter appears localized towards the mid-cell for non-dividing cells, while the ter in dividing cells appears to be in mostly the same location as the oriC, centered in each individual cell before binary fission. In non-dividing cells, the focus is localized slightly away from the mid-cell (sub-polar). In dividing cells, the foci appear to be centrally localized in each dividing cell right before binary fission. The clear splitting of one focus to two foci, like the oriC, indicates that the chromosomes are segregated along the long axis of the cell, there is one chromosome, and *M. smithii* is monoploid.

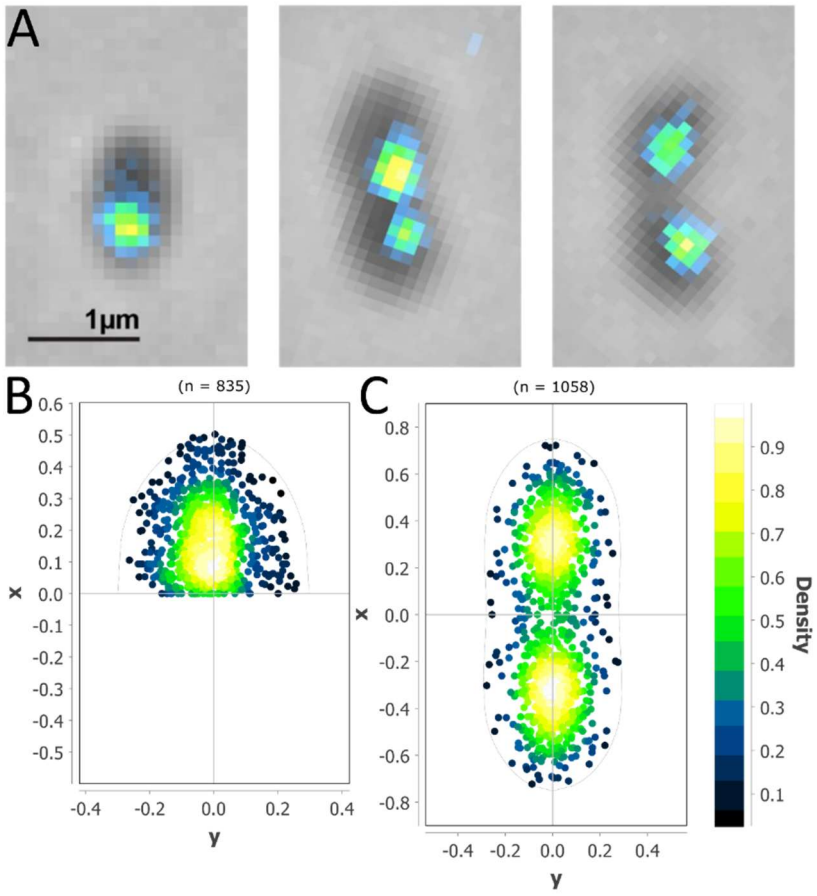

Figure 16 RASER-FISH quantitative analysis of fluorescent maxima of the *xera* region in *M. smithii*. The x and y axes show the relative position of fluorescent foci within a cell. The more yellow/white, the higher the number of foci in a certain location, with white (1.0) being the highest density of foci. The cell outline represents the mean cell outline from all the cells. In (B) are the foci of non-dividing cells and in (C) are the foci of dividing cells. (n) indicates the cell number in which the fluorescent maxima were detected. Representative image by Nika Pende.

The representative image for the ter looked the same for both Direct-geneFISH and RASER-FISH (Figure 16A). We performed the same analysis using the RASER-FISH results, which supports the Direct-geneFISH results. One can see, like from the oriC RASER-FISH quantitative analysis results (Figure 15B & C), that the foci are seen more concentrated within the cell and that the foci are more clustered in the RASER-FISH quantitative analysis plots than in the Direct-geneFISH quantitative analysis plots (Figure 15B & C, Figure 16B & C). Unlike the oriC results, the quantitative analysis for both the Direct-geneFISH and RASER-FISH results look very similar, with no major differences to overall foci localization patterns.

qPCR of the *cdc6* gene furthers evidence of monoploidy

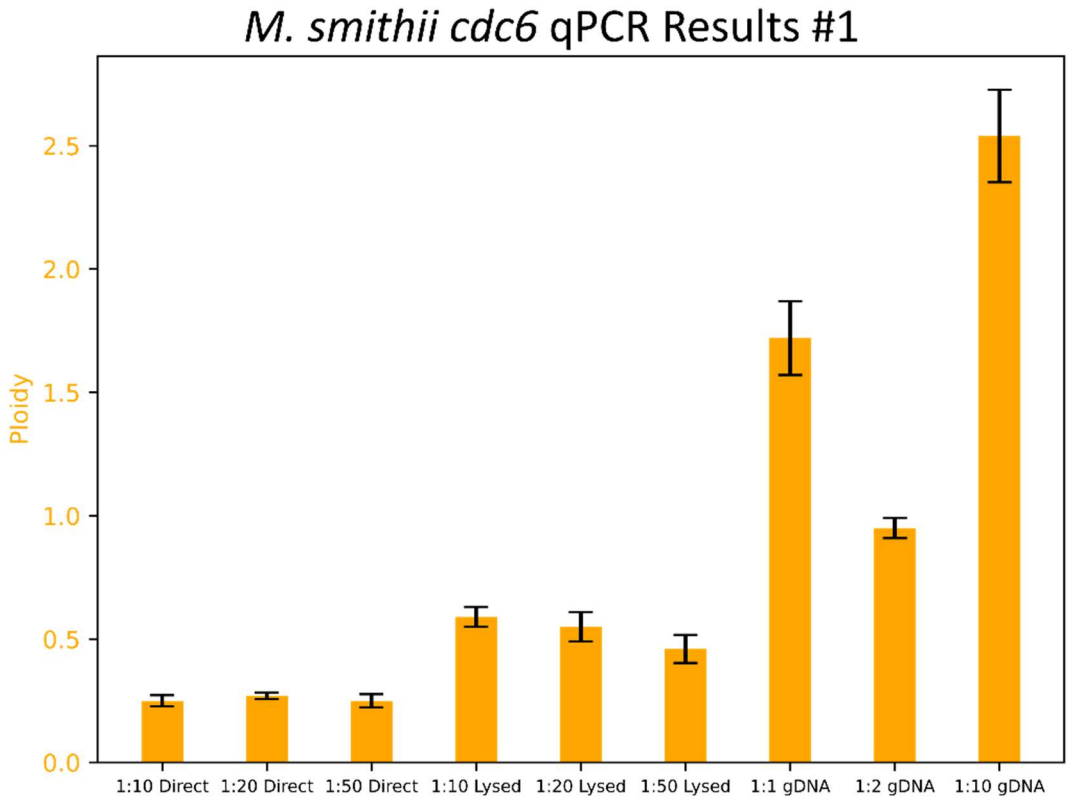

Figure 17 First set of qPCR results of *M. smithii cdc6*. The graph shows ploidy plotted on the y-axis for different samples plotted on the x-axis. Error bars show standard deviation of triplicate cell count and triplicate qPCR reactions.

The first qPCR had an efficiency of 96.5%, a slope of -3.41, and an R^2 of 0.999. We used a gDNA concentration of 277.38 ng/µL for the following reactions.

We can observe that the cells directly added to the qPCR reactions had low efficiency, lysed cells had moderate efficiency, and gDNA had high efficiency (Figure 17). The data is somewhat inconclusive, due to the large range of ploidy levels between the samples. However, the direct and lysed cells indicate that *M. smithii* is at most monoploid. The gDNA, on the other hand, indicates *M. smithii* could be between monoploid or diploid. The error is much higher for the gDNA than the direct or lysed cells, so it could be less reliable. From the qPCR data and the bioinformatic and microscopy data, we can infer that *M. smithii* is most likely monoploid.

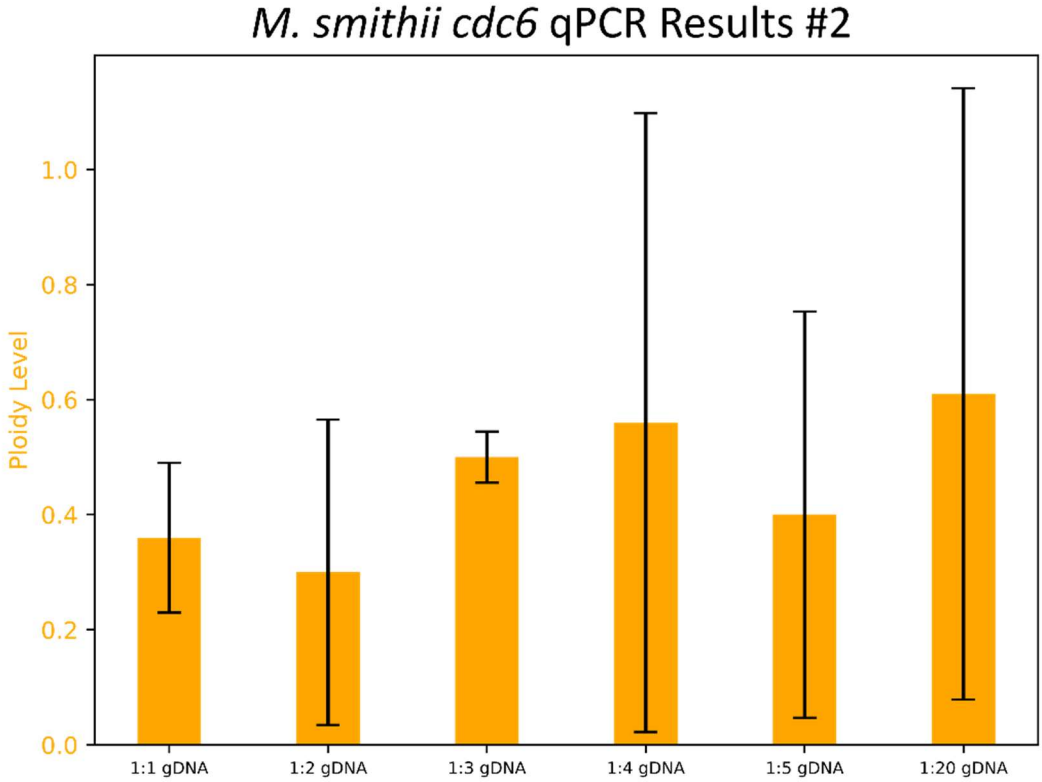

Figure 18 Second set of qPCR results of *M. smithii cdc6*. The graph shows ploidy plotted on the y-axis for different samples plotted on the x-axis. Error bars show standard deviation of triplicate cell count and triplicate qPCR reactions.

The second qPCR had an efficiency of 92.41%, a slope of -3.52, and an R^2 of 0.998. We used a gDNA concentration of 277.38 ng/µL for the following reactions.

We can observe that the second qPCR, with only gDNA run as the template, shows the ploidy of *M. smithii* to be, at most, monoploid (Figure 18). We can observe that the error is very high, so these results are inconclusive. There appears to be no significant difference between ploidy of the different concentrations.

M. kandleri results

MFA-based prediction of *M. kandleri* ori

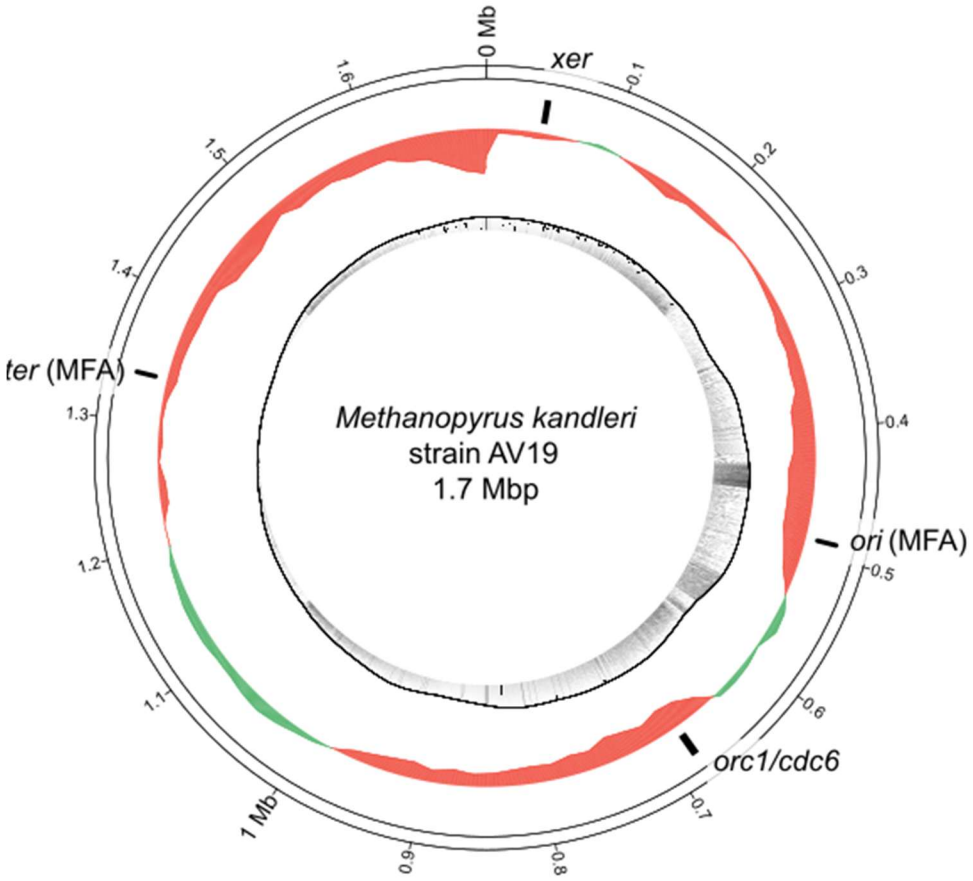

Figure 19 Genome map of *M. kandleri* with GenSkew and MFA results. The GC skew values based on the Genskew analysis (green/red), and the marker frequency analysis (MFA) results (gray) are mapped on the *M. kandleri* genome. The genes associated with oriC (*orc1/cdc6*) and the ter (*xera*) are also shown for reference. The outer ring shows the genome size in megabases (Mb). The central ring shows the results of the GenSkew, with green indicating the GC skew of the leading and red showing GC skew of the lagging strand in the genome, with the amount of skew indicated by the peaks. The inner ring shows the results of the MFA. Image and analysis by Tobias Viehboeck.

For *M. kandleri*, we could not determine the oriC and ter using GenSkew but we obtained results using MFA. The MFA results show the oriC at around 0.49 Mb and the ter at around 1.34 Mb (Figure 19). We can see this in the graph, with the read number highest at and near the oriC and lowest at the ter. We only found one oriC and ter using MFA, so we can confirm that there is only one oriC for each chromosome of *M. kandleri*.

DNA staining indicates polyploidy

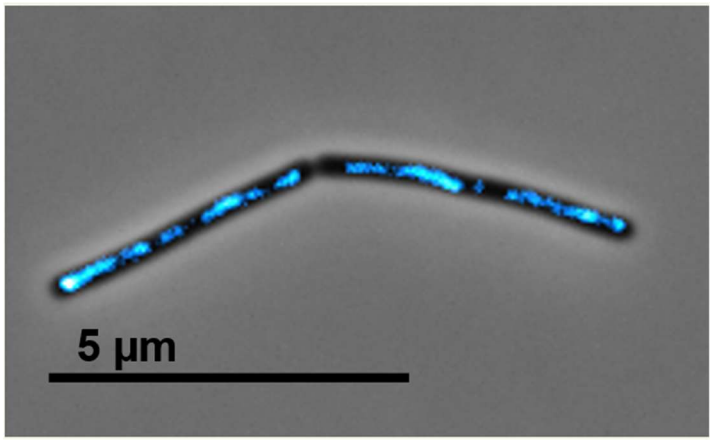

Figure 20 Representative image of *M. kandleri* cells stained with Hoechst.

Figure 20 show preliminary DNA staining of *M. kandleri* with Hoechst.

Discussion

GenSkew and MFA

We were able to obtain GenSkew results for *M. smithii*, however, the ori and ter were not found opposite of each other and rather far awa from each other (Figure 11). This does not correspond with the current literature, which indicates that the ori and ter are typically opposite from each other, as found in bacteria, which archaea have many similarities to (Cortez et al., 2010; Louarn et al., 1977; Reyes-Lamothe et al., 2012). The MFA results for *M. smithii* were more aligned with current knowledge, showing the ori and ter opposite of each other. Still, the MFA showed the ori and ter at different positions than the genes associated with them, which was not ideal (Figure 11). It is possible the MFA locations reflect the true locations of the ori and ter, but it could also be false, as we should expect the ori and ter associated genes to be close to the ori and ter (Bell, 2017; Blakely et al., 1991, 1993; Clerget, 1991). We therefore decided to use the gene locations to produce the probes and perform the DNA FISH experiments.
For *M. kandleri*, we were unable to obtain the location of the ori and ter using GenSkew, although we still got a resulting graph (Figure 19). These results could not be used and we had to perform MFA instead. The MFA results were good, with the ori and ter almost exactly opposite of each other. We compared these results to the location of the ori and ter associated genes, like for *M. smithii*. This time, the genes were not opposite from each other and not close to the MFA determined locations of the ori and ter. We did not have time to run the RASER-FISH experiment for *M. kandleri*, but it was established that we would use the MFA determined ori and ter locations to produce the probes around, since the genes did not seem to correspond as well as the MFA results, unlike for *M. smithii*.

Hoechst staining

We obtained Hoechst staining for *M. smithii* and good results from the quantitative analysis. We were able to clearly see where the DNA was localized in representative image and the quantitative analysis. With the information, we predicted that *M. smithii* could be monoploid, as DNA localization can indicate this. Extracting conclusions from DNA staining is, however, speculative and further experiments are required. Past research using flow-cytometry and DAPI staining, an automated approach to Hoechst staining, have been used to determine the ploidy, however, this has been be a consistent method, which was clear with earlier studies on *Azotobacter vinelandii* (Maldonado et al., 1992, 1994; Nagpal et al., 1989).

We also obtained good Hoechst staining for *M. kandleri*, however, due to time constraints, could not perform a quantitative analysis.

Direct-geneFISH

Results

We obtained excellent results for *M. smithii* using Direct-geneFISH. During imaging, we were able to get good signal and very good penetration of the probes into a large number of cells. The cells did not look to be damaged by the heat denaturation and there was good cell separation on the slide. For the quantitative analysis, due to good cell separation, most of the cells were detected automatically by the MicrobeJ software. Only a small number of cells required outline adjustments or to be removed during manual adjustment for the analysis.

Optimization of Direct-geneFISH

Although excellent results were obtained, we had to make many protocol optimizations. We had to adjust the following parameters: PEIW concentration for permeabilization, formamide concentration in the hybridization buffer, fixation solution and percentage (methanol/formaldehyde), and the concentration of the fluorescently labeled probe used.

PEIW is a phage endoisopeptidase that was shown to permeabilize the cell wall of *M. smithii* (Pende & Sogues et al., 2021). This enzyme is not commercially available, but the we made a plasmid expressing the *PEIW* gene and its purifying the protein. Therefore, the amounts and quality of the PEIW varied. We tried several different PEIW concentrations to enhance permeability of the probe within the cells. Too much or too little resulted in no penetration or lysis of the cell, respectively. We ultimately used 15 µL of PEIW (0.59 mg/mL) in 85 µL of buffer, for a 15% PEIW concentration.

We tried several formamide concentrations to enhance the specificity of the probes to the DNA to improve signal and at the same time to reduce background signal (Barrero-Canosa & Moraru, 2021). We ended up using 15% formamide in our hybridization buffer.

We tried both 80% methanol and 4% formaldehyde for fixation. While methanol fixation also permeabilizes the cells some, formaldehyde was better at crosslinking the DNA. This resulted in 80% methanol resulting in better hybridization of the probes, while 4% formaldehyde provided better DNA staining with Hoechst. The DNA staining with 80% methanol fixed cells was much worse, since both the signal and the percentage of cells stained were lower than with formaldehyde fixed cells. We ultimately used 80% methanol fixation to get better probe signal at the cost of DNA staining signal.

We tried various concentrations of the labeled probe to get stronger fluorescence signal. We ultimately used the highest amount recommended in the original protocol (Barrero-Canosa & Moraru, 2021) of 600 pg/µL since the signal was still weak even with this concentration.

We also tried to improve cell separation to improve imaging and analysis. This was done by adding 0.1% PBS-T, where the 0.1% of the gentle detergent Tween 20 helps prevent cell aggregation after permeabilization. Additionally, we tested different lengths of sonication inside a sonication bath to help separate cells before drying to the slide. We also tested using a sonication tip, at low settings, to separate the cells, however, this was too strong and could damage the cells.

RASER-FISH

Results

As for the Direct-geneFISH, we obtained excellent results for *M. smithii* using RASER-FISH. While imaging, we were able to get excellent signal, which was noticeably better than the Direct-geneFISH, and very good penetration of the probes into a large number of cells. The cells looked the same as the those from the heat denaturation. It is, however, possible that the heat denaturation quenched the fluorescent signal of the probes (Baker, 2005), resulting in the difference in signal between the two FISH methods. For the quantitative analysis, due to good cell separation, most of the cells were detected automatically by the MicrobeJ software. The cell separation was even better than from Direct-geneFISH as a result of switching the Triton X-100 for the last step before drying the cells onto the slide. Again, only a small number of cells required outline adjustments or to be removed during manual adjustment for the analysis.

Optimization of RASER-FISH

Most of the parameters used for RASER-FISH were optimized during optimization of Direct-geneFISH. However, we made optimizations to the hybridization buffer and fixation solution.

For fixation, we tried 100% methanol since this was the recommendation from the original RASER-FISH protocol (Brown et al., 2022). We also used the 80% methanol fixation used for Direct-geneFISH as comparison.

A simplified 50% formamide hybridization buffer was recommended for RASER-FISH, so we tried using this first. This buffer did not have a few components from the Direct-geneFISH hybridization buffer which were sheared salmon sperm DNA, yeast RNA, and DNA blocking reagent. Likely as a result, this buffer did not work at all, with a lot of noise during imaging, and no specific probe signal. This is probably because the buffer was optimized for eukaryotic cells, as this protocol was initially developed for them. We therefore tried the 15% Direct-geneFISH hybridization buffer which worked well and provided excellent results during the first trial.

Comparison of FISH methods

From the results and during execution of the method, we established that RASER-FISH is better than Direct-geneFISH. In the quantitative analysis we can see that the foci are more closely clustered at the highest density point using RASER-FISH compared to Direct-geneFISH (Figure 13, Figure 14, Figure 15 & Figure 16). We think this is because the heat denaturation quenches the fluorescent signal of the FISH probes, since the fluorescent signal was much stronger while imaging for RASER-FISH compared to Direct-geneFISH. This resulted in better detection of foci and probe signal. We observed this higher fluorescence to make RASER-FISH a better method, along with its potential to not damage cells during hybridization, even though it was not observed with our archaeon—it cannot be universally applied that all cells will do so well under the heat of Direct-geneFISH, as *M. smithii* cells showed high resilience during experimentation.

qPCR

Results

We used qPCR instead of earlier methods like flow cytometry, since the latter has proven to be unreliable (Breuert et al., 2006). This approach, however, is still being explored for a wider range of archaea, therefore, we obtained mixed results for the qPCR of *M. smithii*. We were able to test different methods of adding the template DNA to the qPCR reactions, which yielded clear results (Figure 17), but it was not as clear as expected in-terms of the ploidy determined. Looking at the individual results for the direct and lysed cells and gDNA, a clear pattern cannot be seen, but taken together, a pattern emerges. We observed a stepwise increase in the ploidy going from what we believed would be the least efficient to most efficient amplification, suggesting that there are efficiency differences. We could clearly see that the ploidy calculated was lower for direct cells, which likely have inhibitors of the qPCR still inside. Adding the cells directly also results in a delay before the cells lysed and the DNA is exposed for amplification by the primers. Adding in lysed cells worked slightly better, as the ploidy calculation went up. Compared now to the gDNA, a major difference was observed. This showed that the gDNA was the most efficient, which makes sense, as the gDNA is the quickest to be amplified as there is no issue with access to the gDNA as is for the other methods. This establishes that the gDNA should be extracted and that this is the method to use for running the qPCR. This was also the method determined to be the

best the ploidy study on *H. salinarum*, where a phenol-chloroform extract was also performed (Breuert et al., 2006).

Regarding the ploidy, the results indicated the ploidy from just the qPCR, however not definitively. Having the results from the FISH experiments helped us to assume that *M. smithii* is monoploid and that these qPCR results reinforce this. The results of the first set of qPCR results with gDNA vs the direct and lysed cells showed that the ploidy was on average 1.5 for the gDNA, 0.5 for the lysed, and 0.3 for the direct cells (Figure 17). For the second results, the gDNA at different dilutions resulted in a ploidy, on average, of 0.5. These large variations in the results, particularly between the gDNA of the two sets, require questioning of the reliability of the results. We also are skeptical due to a large standard deviations for the first set of results and extraordinarily large standard deviations for the second set, which are not good error levels for the results (Livingston, 2004). Nevertheless, we can infer from the qPCR results, that *M. smithii* is at least not polyploid. From the first set of results it could be inferred that *M. smithii* is diploid, but the FISH results lead us to conclude that *M. smithii* is monoploid. This is reinforced by the fact that most of the qPCR results have a ploidy of around 0.5 rather than 2. Since the ploidy cannot be 0, we would round up to 1. Since the qPCR was not fully optimized, due to time constraints, we can assume there are unaccounted factors like PCR inhibitors (Lance & Guan, 2020; Sidstedt et al., 2020) or gDNA extraction inefficiencies (Demeke & Jenkins, 2010) that result in the copy number not exactly corresponding to the cell count.

Optimization of qPCR

We made many optimizations to the qPCR and with some still needing to be performed, which due to time limitations could not be done. We had to optimize several methods such as: gDNA extraction, cell counting, template amount, and template type. The qPCR method is extremely sensitive to any inefficiencies in gDNA extraction, mistakes in cell counting, and inefficiencies during the qPCR.

We did a lot of optimizations of the gDNA extraction, including testing and comparing several methods that we ultimately did not use for the final experiments shown in the results, which ended up being phenol-chloroform extraction. We also used the DNA Power Soil kit by Qiagen and a feces DNA kit by Promega. In-addition to kits, we also tried a method called drop dialysis (Görisch, 1988), where a drop of lysed cells (cleaned and with cell debris removed) floated on a filter floating on water. This allowed the drop to dialyze through the membrane and hopefully resulting in only DNA remaining in the drop and smaller proteins passing through. With comparing the methods, the kits ended up providing very low DNA concentrations compared to the phenol-chloroform, and the drop dialysis was unreliable, even though the measured DNA concentration was higher than the phenol-chloroform extraction. This unreliability was shown when the supposed gDNA was used as a template for PCR and did not yield any results. The curve on the nanodrop was also not good, when measuring the concentration, indicating an issue in quality and possible contaminates remaining in the drop. It was

also very hard to work with the drop, as it could easily be lost or contaminated if the dialysis apparatus was not handled extremely carefully. We attempted these extraction methods to try to get higher efficiency, with hopes that the drop dialysis would work, as this results in no loss of gDNA due to bead beating, like from the phenol-chloroform extraction, or other chemicals and multiple steps, like with the extraction kits.

Ultimately, phenol-chloroform extraction was the easiest and most consistent and reliable method, even though it required a bead beating step where it has been shown that DNA loss can occur (Cullen et al., 2022). In future studies, we would like to pursue a more efficient method of DNA extraction and to measure this, such as using an external DNA recovery standard or competitive qPCR (Mumy & Findlay, 2004).

We also did some optimization with cell counting, as this is another key component of the experiment that can lead to incorrect end results. We first performed only one round of cell counting, but to improve reliability, increased the counting to triplicates. Additionally, we took cell culture three different times from the same culture and used these as the triplicates. The triplicate cell counts were then averaged and used for the ploidy calculation. Additionally, we tested the OD of the culture and then diluted the culture 1:10 for use in cell counting, as it was much quicker and easier to count the cells at a lower density in the counting chamber. To make sure cell counting was reliable, we also cell counted alongside other colleagues and compared counts, to improve the accuracy. Nevertheless, cell counting has still shown to have unavoidable error, with a 5% error when counting for hemoglobin cells (Zhang et al., 2020), due to factors related to the chamber setup and human error. Considering we worked with significantly smaller cells with a different morphology; our error is likely much higher. This was ultimately something that could not be optimized further. We did consider using flow cytometry, as this is the modern way to do highly automated cell counting (Lambrecht et al., 2017), but due to time limitations, we were unable to try this.

The last thing we optimized was both what template we used to amplify the *cdc6* gene and the amount of template. We initially used 1 µL of template for the 20 µL qPCR reaction, but we changed this to 5 µL, as we found this improved the accuracy. This was determined when comparing qPCR results using 1 µL or 5 µL of template. The only downside to doing this was that much more template needed to be prepared for each qPCR. We also tried different templates to see if we could improve the efficiency of the qPCR to get the most accurate data for the ploidy calculation. We tried adding cells directly, like what is done for a colony qPCR. We assumed the cells would lyse during the DNA denaturation step of the qPCR cycle and expose the gDNA for amplification. We recognized that this may not be the most efficient method, since the gDNA is not exposed immediately for amplification and depends on when the cells lyse during the qPCR run. To eliminate this issue, we tried adding cells that were either lysed with sonification, chemically with PEIW, or with slow freezing at -20 °C. Out of these lysing methods, using PEIW was the most reliable, but we were unsure if PEIW would inhibit the qPCR reaction, so we used the second-best method, sonication. This method was

unfortunately not perfect, as sonication led to some loss of cells due to the agitation of the sonicating tip. We also found that the *M. smithii* cells were extremely resilient and a lot of sonication was required, possibly leading to DNA shearing (Sambrook & Russell, 2006), which would alter our results. Since we were unable to fully optimize the lysing procedure, we decided to use gDNA using the phenol-chloroform extraction method developed earlier. With earlier tests, this was showing the highest amplification efficiency, which was indicated by a low Ct/Cq value after a qPCR run, and the most plausible qPCR results. We did not have time to test this thoroughly, but it is also possible that which growth phase (stationary or exponential) the gDNA is extracted from could also have had a large impact on the results. This has been the case with qPCR of other species, which were shown to have an entirely different ploidy depending on which growth phase they are in (Hildenbrand et al., 2011).

The qPCR experiments contained many optimization steps; however, there are further steps that can be improved for future studies. These include the gDNA extraction method, cell counting reliability, and to further investigation on whether there was an alternative to using gDNA as the template.

Conclusion

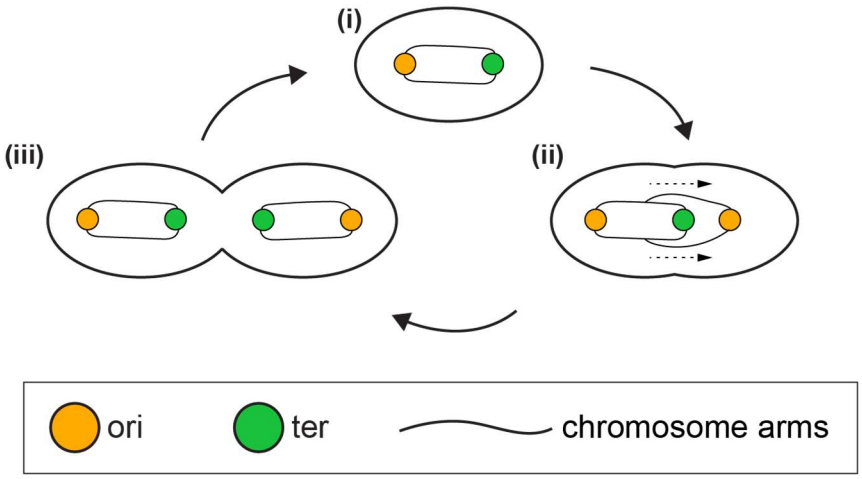

Figure 21 Proposed model of chromosome segregation in *M. smithii*. i) depicts a non-dividing cell, ii) depicts a cell beginning to divide, and iii) shows a cell at the final stage of division before binary fission. Made by Nika Pende.

From the results of the Direct-geneFISH and RASER-FISH results, we have determined that *M. smithii* is monoploid and that the chromosomes segregate longitudinally and we propose a working model shown in Figure 21. We have also observed that the origin and terminus of replication are both near each other on the chromosome and both segregate longitudinally with the chromosome. Furthermore, we observed that in non-dividing cells there is clear polarization of the ori and ter at one third (subpolar).

Lastly, we determined that *M. smithii* is monoploid from these results, as only a singular ori and ter are visible in non-dividing cells but two become visible as the cells divide.

The Direct-geneFISH and RASER-FISH results had no significant differences regarding the ploidy and chromosome segregation results, however, the RASER-FISH results appear to have higher resolution (foci are more tightly clustered at the highest density) in the quantitative analysis than Direct-geneFISH. Additionally, during imaging, the probes had much higher fluorescence within the cells after performing RASER-FISH compared to Direct-geneFISH. This was clear because a much lower exposure time was required to observe good fluorescence while imaging. This suggests that heat denaturation may quench the fluorescence of the probes in Direct-geneFISH, as this is the main difference between the two methods. This relationship has, however, not been established.

Regarding the qPCR, *M. smithii* looks to be monoploid, however, the qPCR results were not reliable, and the experiment requires further optimization. We were, however, able to observe that adding cells directly, adding lysed cells directly, or adding gDNA yielded different results. The cells added directly had the lowest ploidy detected and the gDNA had the highest ploidy detected, while the lysed cells were in-between. The gDNA showed the most accurate results that correspond with the data from the microscopy. This information will help to improve the qPCR in the future.

Outlook

Following the completion of this research, several areas of future research are foreseen for *M. kandleri*. These include RASER-FISH studies, since the origin and terminus of replication were already determined for this purpose. This would also allow the determination of the chromosome configuration and get an idea of the ploidy. RASER-FISH would be used, since it is possibly less damaging to the cells than Direct-geneFISH.

I would also like to refine the qPCR for *M. kandleri*, which was already started. With RASER-FISH data first, optimization would be much easier than it was without it. Lastly, I would like to use higher resolution microscopy like 3D SIM (structured illumination microscopy), to view the spatial orientation of the chromosomes and determine the location of the origin and terminus of replication with more precision. I would also like to perform this on *M. kandleri* after the above experiments are completed.

References

Albers, S.-V., & Meyer, B. H. (2011). The archaeal cell envelope. *Nature Reviews Microbiology*, *9*(6), 414–426. https://doi.org/10.1038/nrmicro2576

Baker, A. (2005). Thermal fluorescence quenching properties of dissolved organic matter. *Water Research*, *39*(18), 4405–4412. https://doi.org/10.1016/j.watres.2005.08.023

Barillà, D. (2016). Driving Apart and Segregating Genomes in Archaea. *Trends in Microbiology*, *24*(12), 957–967. https://doi.org/10.1016/j.tim.2016.07.001

Barrero-Canosa, J., & Moraru, C. (2021). Linking Microbes to Their Genes at Single Cell Level with Direct-geneFISH. In N. F. Azevedo & C. Almeida (Eds.), *Fluorescence In-Situ Hybridization (FISH) for Microbial Cells: Methods and Concepts* (pp. 169–205). Springer US. https://doi.org/10.1007/978-1-0716-1115-9_12

Bell, S. D. (2017). Initiation of DNA Replication in the Archaea. In H. Masai & M. Foiani (Eds.), *DNA Replication: From Old Principles to New Discoveries* (pp. 99–115). Springer. https://doi.org/10.1007/978-981-10-6955-0_5

Bernander, R., & Poplawski, A. (1997). Cell cycle characteristics of thermophilic archaea. *Journal of Bacteriology*, *179*(16), 4963–4969. https://doi.org/10.1128/jb.179.16.4963-4969.1997

Blakely, G., Colloms, S., May, G., Burke, M., & Sherratt, D. (1991). Escherichia coli XerC recombinase is required for chromosomal segregation at cell division. *The New Biologist*, *3*(8), 789–798.

Blakely, G., May, G., McCulloch, R., Arciszewska, L. K., Burke, M., Lovett, S. T., & Sherratt, D. J. (1993). Two related recombinases are required for site-specific recombination at dif and cer in E. coli K12. *Cell*, *75*(2), 351–361. https://doi.org/10.1016/0092-8674(93)80076-Q

Boone, D. R., Whitman, W. B., & Rouvière, P. (1993). Diversity and Taxonomy of Methanogens. In J. G. Ferry (Ed.), *Methanogenesis: Ecology, Physiology, Biochemistry & Genetics* (pp. 35–80). Springer US. https://doi.org/10.1007/978-1-4615-2391-8_2

Breuert, S., Allers, T., Spohn, G., & Soppa, J. (2006). Regulated Polyploidy in Halophilic Archaea. *PLOS ONE*, *1*(1), e92. https://doi.org/10.1371/journal.pone.0000092

Brown, J. M., De Ornellas, S., Parisi, E., Schermelleh, L., & Buckle, V. J. (2022). RASER-FISH: Non-denaturing fluorescence in situ hybridization for preservation of three-dimensional interphase chromatin structure. *Nature Protocols*, *17*(5), 1306–1331. https://doi.org/10.1038/s41596-022-00685-8

Burggraf, S., Stetter, K. O., Rouviere, P., & Woese, C. R. (1991). *Methanopyrus kandleri:* An Archaeal Methanogen Unrelated to all Other Known Methanogens. *Systematic and Applied Microbiology*, *14*(4), 346–351. https://doi.org/10.1016/S0723-2020(11)80308-5

Camara, A., Konate, S., Tidjani Alou, M., Kodio, A., Togo, A. H., Cortaredona, S., Henrissat, B., Thera, M. A., Doumbo, O. K., Raoult, D., & Million, M. (2021). Clinical evidence of the role of Methanobrevibacter smithii in severe acute malnutrition. *Scientific Reports*, *11*(1), 5426. https://doi.org/10.1038/s41598-021-84641-8

Capes, M. D., Coker, J. A., Gessler, R., Grinblat-Huse, V., DasSarma, S. L., Jacob, C. G., Kim, J.-M., DasSarma, P., & DasSarma, S. (2011). The information transfer system of halophilic archaea. *Plasmid*, *65*(2), 77–101. https://doi.org/10.1016/j.plasmid.2010.11.005

Clerget, M. (1991). Site-specific recombination promoted by a short DNA segment of plasmid R1 and by a homologous segment in the terminus region of the Escherichia coli chromosome. *The New Biologist*, *3*(8), 780–788.

Conrad, R. (2009). The global methane cycle: Recent advances in understanding the microbial processes involved. *Environmental Microbiology Reports*, *1*(5), 285–292. https://doi.org/10.1111/j.1758-2229.2009.00038.x

Cortez, D., Quevillon-Cheruel, S., Gribaldo, S., Desnoues, N., Sezonov, G., Forterre, P., & Serre, M.-C. (2010). Evidence for a Xer/dif System for Chromosome Resolution in Archaea. *PLOS Genetics*, *6*(10), e1001166. https://doi.org/10.1371/journal.pgen.1001166

Cullen, J. T., Lawlor, P. G., Cormican, P., Crispie, F., & Gardiner, G. E. (2022). Optimisation of a bead-beating procedure for simultaneous extraction of bacterial and fungal DNA from pig faeces and liquid feed for 16S and ITS2 rDNA amplicon sequencing. *Animal - Open Space*, *1*(1), 100012. https://doi.org/10.1016/j.anopes.2022.100012

Demeke, T., & Jenkins, G. R. (2010). Influence of DNA extraction methods, PCR inhibitors and quantification methods on real-time PCR assay of biotechnology-derived traits. *Analytical and Bioanalytical Chemistry*, *396*(6), 1977–1990. https://doi.org/10.1007/s00216-009-3150-9

Djemai, K., Drancourt, M., & Tidjani Alou, M. (2022). Bacteria and Methanogens in the Human Microbiome: A Review of Syntrophic Interactions. *Microbial Ecology*, *83*(3), 536–554. https://doi.org/10.1007/s00248-021-01796-7

Ducret, A., Quardokus, E. M., & Brun, Y. V. (2016). MicrobeJ, a tool for high throughput bacterial cell detection and quantitative analysis. *Nature Microbiology*, *1*(7), 1–7. https://doi.org/10.1038/nmicrobiol.2016.77

Duggin, I. G., McCallum, S. A., & Bell, S. D. (2008). Chromosome replication dynamics in the archaeon *Sulfolobus acidocaldarius*. *Proceedings of the National Academy of Sciences*, *105*(43), 16737–16742. https://doi.org/10.1073/pnas.0806414105

Garcia, J.-L., Patel, B. K. C., & Ollivier, B. (2000). Taxonomic, Phylogenetic, and Ecological Diversity of Methanogenic *Archaea*. *Anaerobe*, *6*(4), 205–226. https://doi.org/10.1006/anae.2000.0345

Ghavami, S. B., Rostami, E., Sephay, A. A., Shahrokh, S., Balaii, H., Aghdaei, H. A., & Zali, M. R. (2018). Alterations of the human gut *Methanobrevibacter smithii* as a biomarker for inflammatory bowel diseases. *Microbial Pathogenesis*, *117*, 285–289. https://doi.org/10.1016/j.micpath.2018.01.029

Görisch, H. (1988). Drop dialysis: Time course of salt and protein exchange. *Analytical Biochemistry*, *173*(2), 393–398. https://doi.org/10.1016/0003-2697(88)90205-9

Grogan, D. W. (1989). Phenotypic characterization of the archaebacterial genus Sulfolobus: Comparison of five wild-type strains. *Journal of Bacteriology*, *171*(12), 6710–6719. https://doi.org/10.1128/jb.171.12.6710-6719.1989

Hildenbrand, C., Stock, T., Lange, C., Rother, M., & Soppa, J. (2011). Genome Copy Numbers and Gene Conversion in Methanogenic Archaea. *Journal of Bacteriology*, *193*(3), 734–743. https://doi.org/10.1128/jb.01016-10

Huber, H., & Stetter, K. O. (1998). Hyperthermophiles and their possible potential in biotechnology. *Journal of Biotechnology*, *64*(1), 39–52. https://doi.org/10.1016/S0168-1656(98)00102-3

Huber, R., Kurr, M., Jannasch, H. W., & Stetter, K. O. (1989). A novel group of abyssal methanogenic archaebacteria (Methanopyrus) growing at 110 °C. *Nature*, *342*(6251), 833–834. https://doi.org/10.1038/342833a0

Kandler, O., & Konig, H. (1993). Chapter 8 Cell envelopes of archaea: Structure and chemistry. In M. Kates, D. J. Kushner, & A. T. Matheson (Eds.), *New Comprehensive Biochemistry* (Vol. 26, pp. 223–259). Elsevier. https://doi.org/10.1016/S0167-7306(08)60257-4

Kiener, A., König, H., Winter, J., & Leisinger, T. (1987). Purification and use of Methanobacterium wolfei pseudomurein endopeptidase for lysis of Methanobacterium thermoautotrophicum. *Journal of Bacteriology*, *169*(3), 1010–1016. https://doi.org/10.1128/jb.169.3.1010-1016.1987

Konisky, J. (1989). Methanogens for biotechnology: Application of genetics and molecular biology. *Trends in Biotechnology*, *7*(4), 88–92. https://doi.org/10.1016/0167-7799(89)90005-X

Kowalski, D., & Eddy, M. J. (1989). The DNA unwinding element: A novel, cis-acting component that facilitates opening of the Escherichia coli replication origin. *The EMBO Journal*, *8*(13), 4335–4344. https://doi.org/10.1002/j.1460-2075.1989.tb08620.x

Kubota, K., Imachi, H., Kawakami, S., Nakamura, K., Harada, H., & Ohashi, A. (2008). Evaluation of enzymatic cell treatments for application of CARD-FISH to methanogens. *Journal of Microbiological Methods*, *72*(1), 54–59. https://doi.org/10.1016/j.mimet.2007.10.006

Kumar, S., Dagar, S. S., Mohanty, A. K., Sirohi, S. K., Puniya, M., Kuhad, R. C., Sangu, K. P. S., Griffith, G. W., & Puniya, A. K. (2011). Enumeration of methanogens with a focus on fluorescence in situ hybridization. *Naturwissenschaften*, *98*(6), 457–472. https://doi.org/10.1007/s00114-011-0791-2

Kurr, M., Huber, R., König, H., Jannasch, H. W., Fricke, H., Trincone, A., Kristjansson, J. K., & Stetter, K. O. (1991). Methanopyrus kandleri, gen. And sp. Nov. Represents a novel group of hyperthermophilic methanogens, growing at 110°C. *Archives of Microbiology*, *156*(4), 239–247. https://doi.org/10.1007/BF00262992

Lambrecht, J., Cichocki, N., Hübschmann, T., Koch, C., Harms, H., & Müller, S. (2017). Flow cytometric quantification, sorting and sequencing of methanogenic archaea based on F420 autofluorescence. *Microbial Cell Factories*, *16*(1), 180. https://doi.org/10.1186/s12934-017-0793-7

Lance, R. F., & Guan, X. (2020). Variation in inhibitor effects on qPCR assays and implications for eDNA surveys. *Canadian Journal of Fisheries and Aquatic Sciences*, *77*(1), 23–33. https://doi.org/10.1139/cjfas-2018-0263

Leigh, J. A., Albers, S.-V., Atomi, H., & Allers, T. (2011). Model organisms for genetics in the domain Archaea: Methanogens, halophiles, Thermococcales and Sulfolobales. *FEMS Microbiology Reviews*, *35*(4), 577–608. https://doi.org/10.1111/j.1574-6976.2011.00265.x

Lindås, A.-C., & Bernander, R. (2013). The cell cycle of archaea. *Nature Reviews Microbiology*, *11*(9), 627–638. https://doi.org/10.1038/nrmicro3077

Liu, Y., & Whitman, W. B. (2008). Metabolic, Phylogenetic, and Ecological Diversity of the Methanogenic Archaea. *Annals of the New York Academy of Sciences*, *1125*(1), 171–189. https://doi.org/10.1196/annals.1419.019

Livingston, E. H. (2004). The mean and standard deviation: What does it all mean? *Journal of Surgical Research*, *119*(2), 117–123. https://doi.org/10.1016/j.jss.2004.02.008

Louarn, J., Patte, J., & Louarn, J.-M. (1977). Evidence for a fixed termination site of chromosome replication in *Escherichia coli* K12. *Journal of Molecular Biology*, *115*(3), 295–314. https://doi.org/10.1016/0022-2836(77)90156-5

Lundgren, M., Andersson, A., Chen, L., Nilsson, P., & Bernander, R. (2004). Three replication origins in Sulfolobus species: Synchronous initiation of chromosome replication and asynchronous termination. *Proceedings of the National Academy of Sciences*, *101*(18), 7046–7051. https://doi.org/10.1073/pnas.0400656101

Lundgren, M., Malandrin, L., Eriksson, S., Huber, H., & Bernander, R. (2008). Cell Cycle Characteristics of Crenarchaeota: Unity among Diversity. *Journal of Bacteriology*, *190*(15), 5362–5367. https://doi.org/10.1128/jb.00330-08

Luo, Y., Pfister, P., Leisinger, T., & Wasserfallen, A. (2002). Pseudomurein endoisopeptidases PEIW and PEIP, two moderately related members of a novel family of proteases produced in Methanothermobacter strains. *FEMS Microbiology Letters*, *208*(1), 47–51. https://doi.org/10.1111/j.1574-6968.2002.tb11059.x

Mackiewicz, P., Zakrzewska-Czerwińska, J., Zawilak, A., Dudek, M. R., & Cebrat, S. (2004). Where does bacterial replication start? Rules for predicting the oriC region. *Nucleic Acids Research*, *32*(13), 3781–3791. https://doi.org/10.1093/nar/gkh699

Majerník, A. I., Lundgren, M., McDermott, P., Bernander, R., & Chong, J. P. J. (2005). DNA Content and Nucleoid Distribution in Methanothermobacter thermautotrophicus. *Journal of Bacteriology*, *187*(5), 1856–1858. https://doi.org/10.1128/jb.187.5.1856-1858.2005

Malandrin, L., Huber, H., & Bernander, R. (1999). Nucleoid Structure and Partition in Methanococcus jannaschii: An Archaeon With Multiple Copies of the Chromosome. *Genetics*, *152*(4), 1315–1323. https://doi.org/10.1093/genetics/152.4.1315

Maldonado, R., Garzón, A., Dean, D. R., & Casadesús, J. (1992). Gene dosage analysis in Azotobacter vinelandii. *Genetics*, *132*(4), 869–878. https://doi.org/10.1093/genetics/132.4.869

Maldonado, R., Jiménez, J., & Casadesús, J. (1994). Changes of ploidy during the Azotobacter vinelandii growth cycle. *Journal of Bacteriology*, *176*(13), 3911–3919. https://doi.org/10.1128/jb.176.13.3911-3919.1994

Matsunaga, F., Forterre, P., Ishino, Y., & Myllykallio, H. (2001). In vivo interactions of archaeal Cdc6/Orc1 and minichromosome maintenance proteins with the

replication origin. *Proceedings of the National Academy of Sciences*, *98*(20), 11152–11157. https://doi.org/10.1073/pnas.191387498

Maurer, S., Ludt, K., & Soppa, J. (2017). Characterization of Copy Number Control of Two Haloferax volcanii Replication Origins Using Deletion Mutants and Haloarchaeal Artificial Chromosomes. *Journal of Bacteriology*, *200*(1), 10.1128/jb.00517-17. https://doi.org/10.1128/jb.00517-17

Mbakwa, C. A., Penders, J., Savelkoul, P. H., Thijs, C., Dagnelie, P. C., Mommers, M., & Arts, I. C. W. (2015). Gut colonization with methanobrevibacter smithii is associated with childhood weight development. *Obesity*, *23*(12), 2508–2516. https://doi.org/10.1002/oby.21266

Miller, T. L., & Wolin, M. J. (1986). Methanogens in human and animal intestinal Tracts. *Systematic and Applied Microbiology*, *7*(2), 223–229. https://doi.org/10.1016/S0723-2020(86)80010-8

Moissl-Eichinger, C., Pausan, M., Taffner, J., Berg, G., Bang, C., & Schmitz, R. A. (2018). Archaea Are Interactive Components of Complex Microbiomes. *Trends in Microbiology*, *26*(1), 70–85. https://doi.org/10.1016/j.tim.2017.07.004

Mullakhanbhai, M. F., & Larsen, H. (1975). Halobacterium volcanii spec. Nov., a Dead Sea halobacterium with a moderate salt requirement. *Archives of Microbiology*, *104*(1), 207–214. https://doi.org/10.1007/BF00447326

Mumy, K. L., & Findlay, R. H. (2004). Convenient determination of DNA extraction efficiency using an external DNA recovery standard and quantitative-competitive PCR. *Journal of Microbiological Methods*, *57*(2), 259–268. https://doi.org/10.1016/j.mimet.2004.01.013

Nagpal, P., Jafri, S., Reddy, M. A., & Das, H. K. (1989). Multiple chromosomes of Azotobacter vinelandii. *Journal of Bacteriology*, *171*(6), 3133–3138. https://doi.org/10.1128/jb.171.6.3133-3138.1989

Nakamura, K., Terada, T., Sekiguchi, Y., Shinzato, N., Meng, X.-Y., Enoki, M., & Kamagata, Y. (2006). Application of Pseudomurein Endoisopeptidase to Fluorescence In Situ Hybridization of Methanogens within the Family Methanobacteriaceae. *Applied and Environmental Microbiology*, *72*(11), 6907–6913. https://doi.org/10.1128/AEM.01499-06

Norais, C., Hawkins, M., Hartman, A. L., Eisen, J. A., Myllykallio, H., & Allers, T. (2007). Genetic and Physical Mapping of DNA Replication Origins in Haloferax volcanii. *PLOS Genetics*, *3*(5), e77. https://doi.org/10.1371/journal.pgen.0030077

Pende, N., Sogues, A., Megrian, D., Sartori-Rupp, A., England, P., Palabikyan, H., Rittmann, S. K.-M. R., Graña, M., Wehenkel, A. M., Alzari, P. M., & Gribaldo, S. (2021). SepF is the FtsZ anchor in archaea, with features of an ancestral cell division system. *Nature Communications*, *12*(1), 3214. https://doi.org/10.1038/s41467-021-23099-8

Pfister, P., Wasserfallen, A., Stettler, R., & Leisinger, T. (1998). Molecular analysis of Methanobacterium phage ΨM2. *Molecular Microbiology*, *30*(2), 233–244. https://doi.org/10.1046/j.1365-2958.1998.01073.x

Popławski, A., & Bernander, R. (1997). Nucleoid structure and distribution in thermophilic Archaea. *Journal of Bacteriology*, *179*(24), 7625–7630. https://doi.org/10.1128/jb.179.24.7625-7630.1997

Ren, T., Patel, M. K., & Blok, K. (2008). Steam cracking and methane to olefins: Energy use, CO2 emissions and production costs. *Energy*, *33*(5), 817–833. https://doi.org/10.1016/j.energy.2008.01.002

Reno, M. L., Held, N. L., Fields, C. J., Burke, P. V., & Whitaker, R. J. (2009). Biogeography of the Sulfolobus islandicus pan-genome. *Proceedings of the National Academy of Sciences*, *106*(21), 8605–8610. https://doi.org/10.1073/pnas.0808945106

Reyes-Lamothe, R., Nicolas, E., & Sherratt, D. J. (2012). Chromosome Replication and Segregation in Bacteria. *Annual Review of Genetics*, *46*(Volume 46, 2012), 121–143. https://doi.org/10.1146/annurev-genet-110711-155421

Robinson, J. L., Pyzyna, B., Atrasz, R. G., Henderson, C. A., Morrill, K. L., Burd, A. M., DeSoucy, E., Fogleman, R. E., Naylor, J. B., Steele, S. M., Elliott, D. R., Leyva, K. J., & Shand, R. F. (2005). Growth Kinetics of Extremely Halophilic Archaea (Family Halobacteriaceae) as Revealed by Arrhenius Plots. *Journal of Bacteriology*, *187*(3), 923–929. https://doi.org/10.1128/jb.187.3.923-929.2005

Robinson, N. P., & Bell, S. D. (2005). Origins of DNA replication in the three domains of life. *The FEBS Journal*, *272*(15), 3757–3766. https://doi.org/10.1111/j.1742-4658.2005.04768.x

Robinson, N. P., Blood, K. A., McCallum, S. A., Edwards, P. A., & Bell, S. D. (2007). Sister chromatid junctions in the hyperthermophilic archaeon Sulfolobus solfataricus. *The EMBO Journal*, *26*(3), 816–824. https://doi.org/10.1038/sj.emboj.7601529

Robinson, N. P., Dionne, I., Lundgren, M., Marsh, V. L., Bernander, R., & Bell, S. D. (2004). Identification of Two Origins of Replication in the Single Chromosome of the Archaeon Sulfolobus solfataricus. *Cell*, *116*(1), 25–38. https://doi.org/10.1016/S0092-8674(03)01034-1

Sambrook, J., & Russell, D. W. (2006). Fragmentation of DNA by Sonication. *Cold Spring Harbor Protocols*, *2006*(4), pdb.prot4538. https://doi.org/10.1101/pdb.prot4538

Samuel, B. S., Hansen, E. E., Manchester, J. K., Coutinho, P. M., Henrissat, B., Fulton, R., Latreille, P., Kim, K., Wilson, R. K., & Gordon, J. I. (2007). Genomic and metabolic adaptations of Methanobrevibacter smithii to the human gut. *Proceedings of the National Academy of Sciences*, *104*(25), 10643–10648. https://doi.org/10.1073/pnas.0704189104

Sandman, K., & Reeve, J. N. (2006). Archaeal histones and the origin of the histone fold. *Current Opinion in Microbiology*, *9*(5), 520–525. https://doi.org/10.1016/j.mib.2006.08.003

Serre, M.-C., Arnaout, T. E., Brooks, M. A., Durand, D., Lisboa, J., Lazar, N., Raynal, B., Tilbeurgh, H. van, & Quevillon-Cheruel, S. (2013). The Carboxy-Terminal αN Helix of the Archaeal XerA Tyrosine Recombinase Is a Molecular Switch to Control Site-Specific Recombination. *PLOS ONE*, *8*(5), e63010. https://doi.org/10.1371/journal.pone.0063010

Sidstedt, M., Rådström, P., & Hedman, J. (2020). PCR inhibition in qPCR, dPCR and MPS—mechanisms and solutions. *Analytical and Bioanalytical Chemistry*, *412*(9), 2009–2023. https://doi.org/10.1007/s00216-020-02490-2

Spaans, S. K., van der Oost, J., & Kengen, S. W. M. (2015). The chromosome copy number of the hyperthermophilic archaeon Thermococcus kodakarensis KOD1. *Extremophiles*, *19*(4), 741–750. https://doi.org/10.1007/s00792-015-0750-5

Steenbakkers, P. J. M., Geerts, W. J., Ayman-Oz, N. A., & Keltjens, J. T. (2006). Identification of pseudomurein cell wall binding domains. *Molecular Microbiology*, *62*(6), 1618–1630. https://doi.org/10.1111/j.1365-2958.2006.05483.x

Strong, P. J., Xie, S., & Clarke, W. P. (2015). Methane as a Resource: Can the Methanotrophs Add Value? *Environmental Science & Technology*, *49*(7), 4001–4018. https://doi.org/10.1021/es504242n

Visweswaran, G. R. R., Dijkstra, B. W., & Kok, J. (2010). Two Major Archaeal Pseudomurein Endoisopeptidases: PEIW and PEIP. *Archaea*, *2010*(1), 480492. https://doi.org/10.1155/2010/480492

Wang, H., Peng, N., Shah, S. A., Huang, L., & She, Q. (2015). Archaeal Extrachromosomal Genetic Elements. *Microbiology and Molecular Biology Reviews*, *79*(1), 117–152. https://doi.org/10.1128/mmbr.00042-14

Weber, P. M., Moessel, F., Paredes, G. F., Viehboeck, T., Vischer, N. O. E., & Bulgheresi, S. (2019). A Bidimensional Segregation Mode Maintains Symbiont Chromosome Orientation toward Its Host. *Current Biology*, *29*(18), 3018-3028.e4. https://doi.org/10.1016/j.cub.2019.07.064

White, M. F., & Bell, S. D. (2002). Holding it together: Chromatin in the Archaea. *Trends in Genetics*, *18*(12), 621–626. https://doi.org/10.1016/S0168-9525(02)02808-1

Woese, C. R., & Fox, G. E. (1977). Phylogenetic structure of the prokaryotic domain: The primary kingdoms. *Proceedings of the National Academy of Sciences*, *74*(11), 5088–5090. https://doi.org/10.1073/pnas.74.11.5088

Woese, C. R., Kandler, O., & Wheelis, M. L. (1990). Towards a natural system of organisms: Proposal for the domains Archaea, Bacteria, and Eucarya. *Proceedings of the National Academy of Sciences*, *87*(12), 4576–4579. https://doi.org/10.1073/pnas.87.12.4576

Wu, Z., Liu, J., Yang, H., & Xiang, H. (2014). DNA replication origins in archaea. *Frontiers in Microbiology*, *5*. https://doi.org/10.3389/fmicb.2014.00179

Zhang, M., Gu, L., Zheng, P., Chen, Z., Dou, X., Qin, Q., & Cai, X. (2020). Improvement of cell counting method for Neubauer counting chamber. *Journal of Clinical Laboratory Analysis*, *34*(1), e23024. https://doi.org/10.1002/jcla.23024